Reference-free measurements of the $1s2s2p\,^2P^o_{1/2,3/2} \to 1s^22s\,^2S_{1/2}$ and $1s2s2p\,^4P_{5/2} \to 1s^22s\,^2S_{1/2}$ transition energies and widths in lithiumlike sulfur and argon ions

J. Machado [1,*] Guojie Bian [2,3,†] Nancy Paul [2,‡] M. Trassinelli [4,§] P. Amaro [1,¶] M. Guerra,[1,**] C. I. Szabo [5,††]
A. Gumberidze [6,‡‡] J. M. Isac,[2] J. P. Santos [1,§§] J. P. Desclaux [7,¶¶] and P. Indelicato [2,***]

[1]*Laboratório de Instrumentação, Engenharia Biomédica e Física da Radiação (LIBPhys-UNL), Departamento de Física,
Faculdade de Ciências e Tecnologia, FCT, Universidade Nova de Lisboa, 2829-516 Caparica, Portugal*
[2]*Laboratoire Kastler Brossel, Sorbonne Université, CNRS, ENS, PSL Research University, Collège de France,
Case 74, 4 Place Jussieu, 75005 Paris, France*
[3]*Institute of Atomic and Molecular Physics, Sichuan University, Chengdu 610065, People's Republic of China*
[4]*Institut des NanoSciences de Paris, CNRS, Sorbonne Université, 4 Place Jussieu, 75005 Paris, France*
[5]*Theiss Research, La Jolla, California 92037, USA*
[6]*ExtreMe Matter Institute EMMI and Research Division, GSI Helmholtzzentrum für Schwerionenforschung,
64291 Darmstadt, Germany*
[7]*15 Chemin du Billery, 38360 Sassenage, France*

We have measured the widths and energies of the $1s2s2p\,^2P_{1/2,3/2} \to 1s^22s\,^2S_{1/2}$ transitions in lithiumlike sulfur and argon, as well as the energies of the forbidden $1s2s2p\,^4P_{5/2} \to 1s^22s\,^2S_{1/2}$ $M2$ transition in both elements. All measurements were performed with a double-flat-crystal spectrometer without the use of any reference line. The transition energy measurements have accuracies ranging from 2.3 to 6.4 ppm depending on the element and line intensity. The widths and the intensity ratios of the $1s2s2p\,^2P_{1/2,3/2} \to 1s^22s\,^2S_{1/2}$ lines have also been measured. These are reference-free measurements of transitions in core-excited lithiumlike ions and have an accuracy comparable to the best relative measurements. We have also performed multiconfiguration Dirac-Fock calculations of the widths, energies, and intensity ratios. An extensive comparison between existing experimental results and theory is performed, and Bayesian techniques are employed to extract the energy of the $1s2p^2\,^4P_{1/2} \to 1s^22p\,^2P_{1/2}$ transition in sulfur and identify contaminant transitions.

I. INTRODUCTION

Since the beginning of the spectroscopy of highly charged ions (HCIs), continuous improvement has been made in the accuracy of the measured transition energies across a broad range of elements. Measurements in HCIs have extended the tests of the fundamental theory of the interaction between light and matter in bound systems, known as bound-state quantum

————————

*jfd.machado@fct.unl.pt
†bianguojie@gmail.com
‡npaul@lkb.upmc.fr
§trassinelli@insp.jussieu.fr
¶pdamaro@fct.unl.pt
**mguerra@fct.unl.pt
††csilla.szabo-foster@nist.gov
‡‡A.Gumberidze@gsi.de
§§jps@fct.unl.pt
¶¶jean-paul.desclaux@wanadoo.fr
***Corresponding author: paul.indelicato@lkb.upmc.fr

electrodynamics (BSQED), to the strong-field regime. The most-studied transitions are the $2p \to 1s$ transitions in hydrogenlike and heliumlike ions and the $2p \to 2s$ transitions in heliumlike and lithiumlike ions (see [1] for a complete review). These studies are complementary to the progress made in high-accuracy measurements of transition energies in hydrogen [2–4]. Others fundamental quantities like the Landé g factor in H-like ions such as carbon [5–8], oxygen [9], or silicon (^{28}Si^{13+}) [10,11] and in Li-like ions (^{28}Si^{11+}) [12] and the hyperfine structure have also been measured to provide tests of BSQED [1]. These advances in HCI spectroscopy have also provided important data for the diagnostics of astrophysical, laboratory, and fusion plasmas.

Hydrogenlike ions have been studied across a wide range of elements up to uranium [1,13]. A variety of techniques have been used, such as beam-foil spectroscopy, recoil ions, crystal spectroscopy on fast beams, and radiative electron capture at a storage ring electron cooler. More recently, very accurate reference-free measurements of hydrogenlike ions [14,15] have been reported using crystal spectrometers and highly charged ion sources like electron-beam ion traps (EBITs). Their accuracy is of the order of a few parts per million (ppm), an order of magnitude improvement from previous measurements. The agreement between theory and experiment for one-electron ions is quite satisfactory (see, for example, [16]).

There have also been high-accuracy reference-free measurements of two-electron ions using both EBITs [15,17] and electron cyclotron resonance ion sources (ECRISs) [18,19]. Agreement between measurements in heliumlike ions and QED calculations [20] is also excellent (see Refs. [1,19] for a detailed review of available measurements and a comparison with theory). For three-electron ions there are very accurate measurements and calculations for the $1s^2 2p\,^2P_J \rightarrow 1s^2 2s\,^2S_{1/2}$ transitions, for elements up to very heavy ones like lead, bismuth, thorium, and uranium [21–28] using both EBITs and accelerators. For these systems, overall good agreement is found between all the available experiments and the most advanced calculations [1,29–32].

The situation is very different for transitions in lithiumlike ions with a core-excited initial level, like the $1s2s2p\,^2P_J$ level, often observed as satellites of the heliumlike transitions. A number of measurements have been made, but most of them are relative and not very accurate. Considering just the measurements for $Z \geqslant 10$ and of the transitions labeled q ($1s2s2p\,^2P_{3/2}^o \rightarrow 1s^2 2s\,^2S_{1/2}$) and r ($1s2s2p\,^2P_{1/2}^o \rightarrow 1s^2 2s\,^2S_{1/2}$) by Gabriel [33], we can cite in chronological order several experiments performed for $11 \leqslant Z \leqslant 17$ and K, Ti, and V [34]; Si [35]; Ti [36]; Ar [37]; Sc, V, Cr, and Mn [38]; Ni [39]; V [40]; Ca [41]; Co [42]; Sc [43]; Fe [44]; Ne [45]; Ar [46,47]; Fe [48]; Ar [49]; Fe [50]; S, Cl, and Ar [51]; and Ca [52]. These measurements were performed using laser-generated plasmas [34], beam-foil spectroscopy, and tokamaks. There is only one measurement for $Z > 28$, performed on the Livermore EBIT for the q line of praseodymium ($Z = 59$) [53]. For the $1s2s2p\,^4P_{5/2} \rightarrow 1s^2 2s\,^2S_{1/2}$ transition, its energy has been measured only in Ar [47,54].

Schlesser *et al.* [51] reported high-accuracy (around 1 ppm) measurements of the $1s2s2p\,^2P_J^o \rightarrow 1s^2 2s\,^2S_{1/2}$ transition in lithiumlike sulfur, chlorine, and argon using a spherical-crystal spectrometer and an ECRIS. These measurements are relative to the theoretical predictions of the $M1$ line energy by Artemyev *et al.* [20]. The only available reference-free measurement of a transition from a core-excited autoionizing level is that of the $1s2s^2 2p\,^1P_1 \rightarrow 1s^2 2s^2\,^1S_0$ transition in Be-like argon [19]. The very accurate measurements of several core-excited lines performed using an EBIT and the PETRA III synchrotron radiation facility use K edges of several elements (Mn, Fe, Co, Ni, and Cu) for calibration [50].

The $1s2s2p\,^2P_J^o$ levels can decay either by radiative transitions to a variety of singly and doubly excited levels or by the Auger effect. Yet there is a single Auger transition to the ground state of the corresponding He-like ion. They are thus a good test case for testing the Auger decay theory. In contrast, in core-excited neutral atoms there can be tens of Auger decay channels. Even for the case of the $1s2s^2 2p\,^1P_1 \rightarrow 1s^2 2s^2\,^1S_0$ transition in Be-like ions there are still three possible Auger transitions. Another feature of these lithiumlike ion core-excited states is that, since the initial level is degenerate with a continuum, it is shifted (the so-called Auger shift) [55–58].

Because of the theoretical interest in a better understanding of the QED, correlation, and Auger shift contributions to the initial level energy, we have performed in the present work reference-free measurements of the $1s2s2p\,^2P_J^o \rightarrow 1s^2 2s\,^2S_{1/2}$ and $1s2s2p\,^4P_{5/2} \rightarrow 1s^2 2s\,^2S_{1/2}$ transition energies in sulfur

and argon with accuracies of a few ppm. We have also measured the widths of the lines. The widths of the r and q transitions have been measured only for iron [50].

The experimental method used to make these measurements has been described in Ref. [59]. This method has already been used to measure with few-ppm accuracy the $1s2s\,^3S_1 \rightarrow 1s^2\,^1S_0$ $M1$ line [18] and the $1s2p\,^1P_1 \rightarrow 1s^2\,^1S_0$ transition [19] energies in He-like argon ions. It was also used to measure the $1s2s^2 2p\,^1P_1 \rightarrow 1s^2 2s^2\,^1S_0$ transition energy and width in Be-like argon ions [19]. Accurate calculations of the transition energies and widths performed using the multiconfiguration Dirac-Fock (MCDF) method are also presented.

The article is organized as follows. In Sec. II we briefly describe the experimental setup used in this work and provide a detailed description of the analysis method, which allows us to obtain the energies and widths with their uncertainties. A brief description of the calculations of transition energies and widths is given in Sec. III. Section IV presents a detailed discussion of the experimental results and comparison with theory for both S and Ar lines. A summary is provided in Sec. V.

II. EXPERIMENTAL METHOD AND DATA ANALYSIS

A. Description of the experiment

A detailed description of the experimental method may be found in Refs. [18,19,59]. Here we only recall the main features of the experiment. A double-flat-crystal spectrometer (DCS) is attached to an electron-cyclotron resonance ion source. The optical axis of the spectrometer is aligned with the ECRIS axis. The plasma in the source has a diameter of approximately 30 mm. The plasma is seen from the spectrometer through a copper tube of an inner diameter of 12 mm. The microwave power to create and maintain the plasma is around 300 W. For measuring the transition energies in argon, a mixture of argon gas and oxygen is injected into the source. For sulfur, SF_6 gas and oxygen are used. In the argon measurement, we use the same gas-filled proportional counter as in Ref. [59] to detect the x rays reflected by the second crystal. In the sulfur measurement we use a large-area avalanche photodiode (LAAPD) instead. The LAAPD is mounted on a copper support cooled to approximately $-10\,^\circ$C using a mixture of ethanol and water to reduce thermal electronic noise. Several blocks of copper, cooled in the same way, are used at different hot spots inside the spectrometer to stabilize the temperature. The spectrometer is under vacuum to avoid absorption of the low-energy x rays by air. The stepping motors used by the rotation table are cooled to avoid heat drift. Heating resistors are mounted on the backs of the crystals and connected to a temperature controller with a proportional-integral-derivative controller which is used to stabilize the crystal temperatures.

Between the argon and the sulfur experiment the ECRIS and the spectrometer have to be moved and fully realigned using the procedure described in Ref. [59] because of construction work in the original location. Checks are performed on the intense Be-like argon line $1s2s^2 2p\,^1P_1 \rightarrow 1s^2 2s^2\,^1S_0$ line and the results are found to be in agreement with our earlier measurement [19].
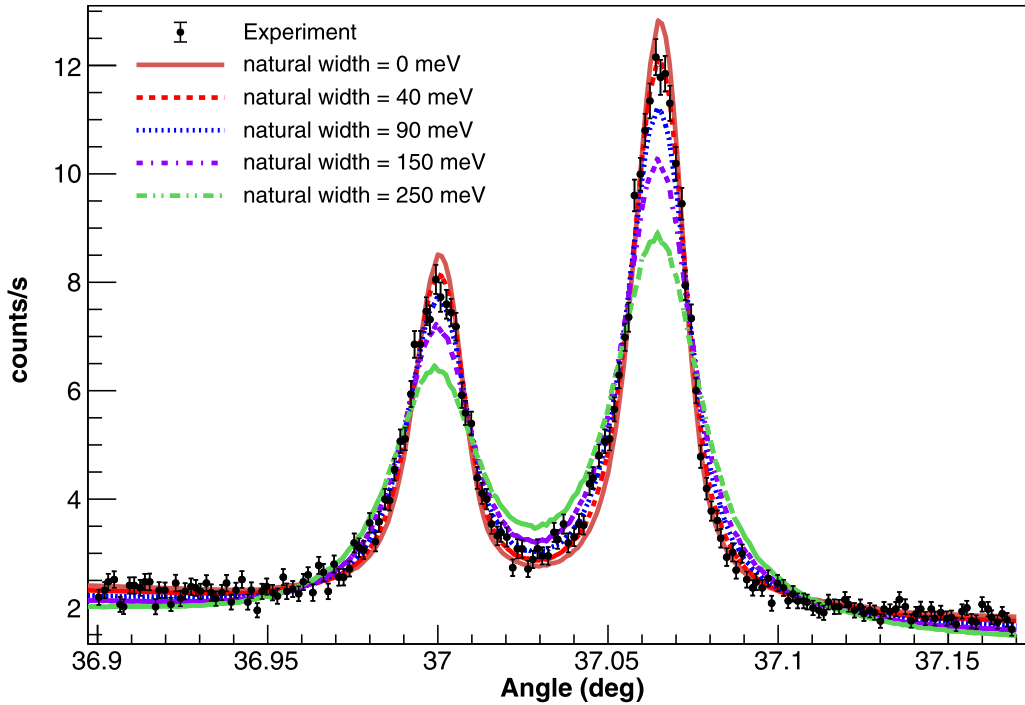
FIG. 1. Example of fits to a dispersive spectrum of the $1s2s2p\,^2P_J \rightarrow 1s^22s\,^2S_{1/2}$, $J = 1/2$, $3/2$ transitions in lithiumlike sulfur. A subset of the simulation spectra with Lorentzian width values $\Gamma_L = 0, 40, 90, 150$, and 250 meV is shown. The error bar for each experimental point is $\sqrt{n}/t$, where n is the number of counts and t the measurement time of the bin.

During the work on argon, the vacuum of the source and that of the spectrometer are separated by a 125-μm-thick Be window. The polarization electrode, which is used to apply a voltage to the plasma to optimize performances and through which the x rays detected by the DCS are passing, has an inner diameter of 12 mm for a length of 300 mm. In the setup used for sulfur, after moving the source, we use a slightly different arrangement with a polarization electrode of the same length, but an inner diameter of 8 mm, identical to the initial design of the SuperNanogan ECRIS we are using, and a 50-μm-thick Be window. The 125-μm-thick Be window has a transmission of 39% at the x-ray energy of lithiumlike sulfur and 64% at the x-ray energy of lithiumlike argon [60]. The 50-μm-thick window has a transmission of 68% and 88%, respectively, partially compensating for the transmission loss due to the smaller electrode diameter. During the measurements on sulfur we find that the source operations are more stable than with argon before, which allows us to obtain more statistics in the sulfur spectra.

B. Data analysis

The data analysis is performed in a similar way as in Ref. [19], yet, in the present case, the dispersive spectra have two lines that are not completely resolved. We thus have to modify the analysis method to obtain the experimental linewidths and energies. We first describe the method for obtaining the linewidths and then how we derived the line energies.

1. Linewidths

A set of simulations is performed using the *ab initio* code described in Ref. [59] for both sulfur and argon. The Doppler width for sulfur is obtained by fitting the He-like $M1$ transition as was done for argon in Ref. [18]. We find $\Gamma_G^{\text{Expt}} = 91.7(74)$ meV. This broadening corresponds to the depth of the trapping well created by the space charge of the electrons in the ECRIS plasma. This depth is approximately 0.2 V [61,62]. For argon we use $\Gamma_G^{\text{Expt}} = 80.5(46)$ meV, the value obtained in [18]. The Lorentzian widths used in the simulation Γ_L^i are taken in the range from 0 to 400 meV. The crystal temperature used in these simulations is $T_{\text{ref}} = 22.5\,^\circ$C. We then proceed as described in Ref. [19]. The nondispersive spectra reflect exactly the response function of the spectrometer and are used to check the result of the simulation. In the nondispersive side, because of the presence of two lines, we have developed a procedure to fit simultaneously the two lines and minimize the χ^2 function. More details on the method and figures can be found in Sec. I A of the Supplemental Material [63]. The error bars are obtained using Eq. (3) of the Supplemental Material following Ref. [64]. Examples of a fitted spectrum with a subset of different Lorentzian widths are shown in Fig. 1 for sulfur and in Fig. 2 for argon. The mean value and the $\pm\sigma$ interval for the pair of widths of the $1s2s2p\,^2P_J \rightarrow 1s^22s\,^2S_{1/2}$ doublet, which we have obtained in this procedure, are presented in Figs. 3 and 4.

For the $1s2s2p\,^4P_{5/2} \rightarrow 1s^22s\,^2S_{1/2}$ transition, the procedure is different. The line is a small well-separated satellite of the $1s2s^22p\,^1P_1 \rightarrow 1s^22s^2\,^1S_0$ transition in berylliumlike sulfur or argon, as shown in Figs. 5 and 6. The natural width of the line is very small as shown in Sec. III. Thus only the Doppler width is used as the linewidth. This is checked by fitting a simulated profile convolved with a Gaussian. The width of the Gaussian is varied and the χ^2 evaluated. The value found is consistent, within the uncertainties,
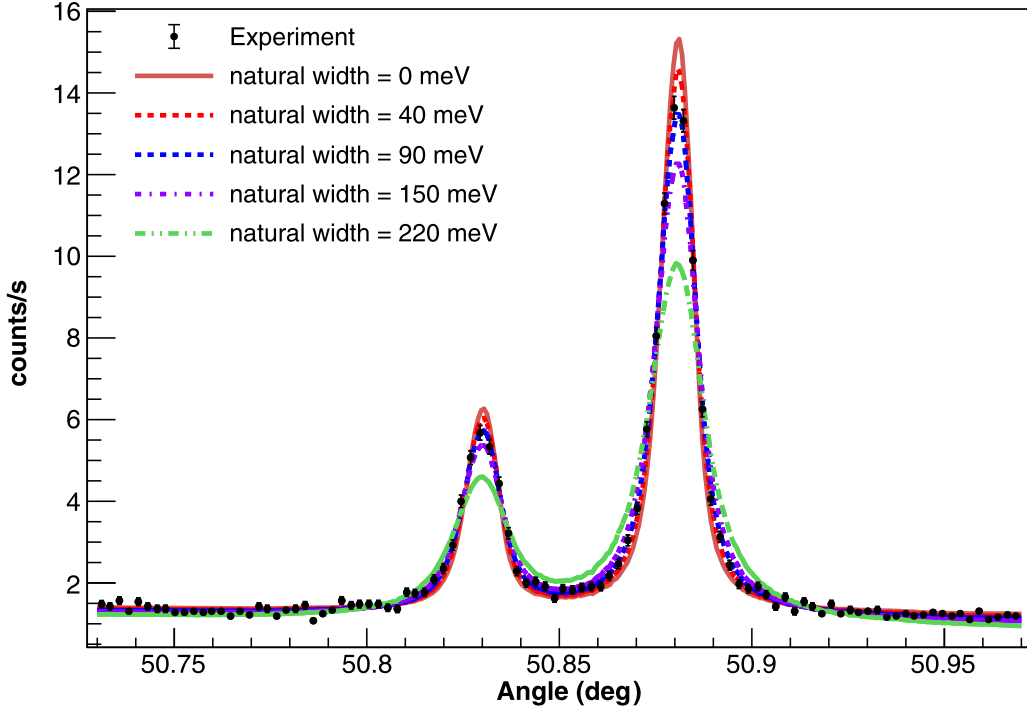
FIG. 2. Example of fits to a dispersive spectrum of the $1s2s2p\,^2P_J \to 1s^22s\,^2S_{1/2}$, $J = 1/2, 3/2$ transitions in lithiumlike argon. A subset of the simulated spectra with Lorentzian width values $\Gamma_L = 0, 40, 90, 150$, and 250 meV is shown. The error bar for each experimental point is $\sqrt{n}/t$, where n is the number of counts and t the measurement time of the bin.

with the Doppler width obtained from the heliumlike $M1$ transition.

2. Transition energies of the $1s2s2p\,^2P_J \to 1s^22s\,^2S_{1/2}$ doublet

For the energy analysis, the method is similar to the one described in Ref. [19]. The difference between the two methods lies in the interpolated functions (constructed by the simulation output), which are fitted to the experimental spectra. For the nondispersive spectrum there is no difference, since there is only one peak for both transitions; however, for the dispersive spectrum, which contains two lines, we calculate fit functions using the two values of the natural widths obtained in the procedure above. We then perform

a spline interpolation of the simulation. The nondispersive spectra obtained from the simulations for both transitions are identical, as they only depend on the angular settings of the spectrometer, which are kept fixed for all simulations. The spline interpolation function in this case is constructed for the dispersive spectrum as

$$
\begin{aligned}
I\big(&\theta - \theta_0^1, \theta - \theta_0^2, I_{\max}^1, I_{\max}^2, a^1, a^2, b^1, b^2\big) \\
&= I_{\max}^1 S_{E_0, \Gamma_L^1, \Gamma_G^{\mathrm{Expt}}, T_{\mathrm{Expt}}}\big(\theta - \theta_0^1\big) \\
&\quad + I_{\max}^2 S_{E_0, \Gamma_L^2, \Gamma_G^{\mathrm{Expt}}, T_{\mathrm{Expt}}}\big(\theta - \theta_0^2\big) + a + b\theta,
\end{aligned} \tag{1}
$$

where the superscripts 1 and 2 represent the two lines in the spectrum, $I_{\max}^1$ and $I_{\max}^2$ represent the line intensities, θ

(a)

(b)
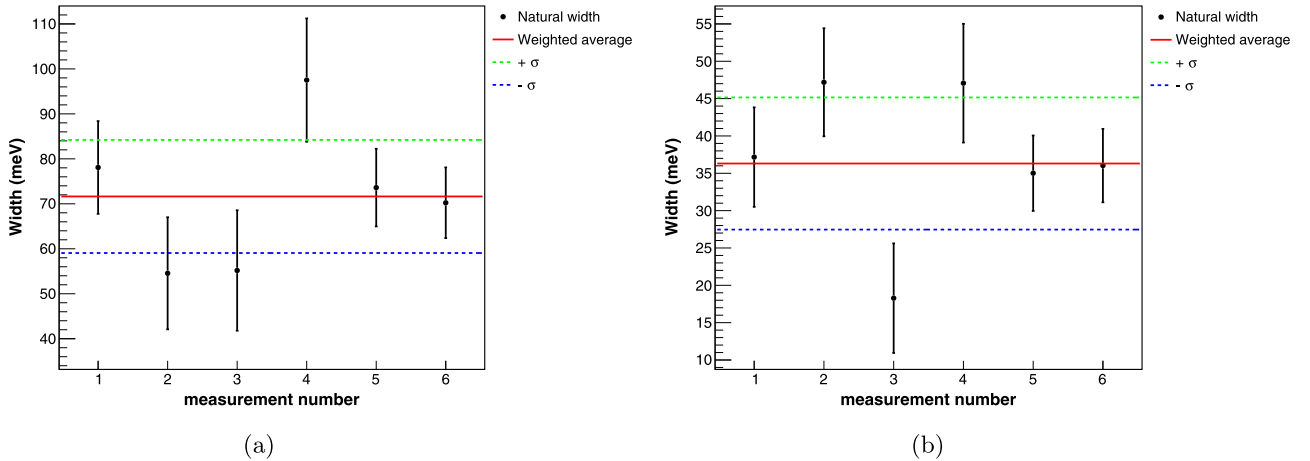
FIG. 3. Natural widths of all spectra recorded during the measurement of the (a) $1s2s2p\,^2P_{1/2} \to 1s^22s\,^2S_{1/2}$ and (b) $1s2s2p\,^2P_{3/2} \to 1s^22s\,^2S_{1/2}$ Li-like sulfur transitions. The weighted average and the 68% confidence interval ($\pm 1\sigma$) are also shown.
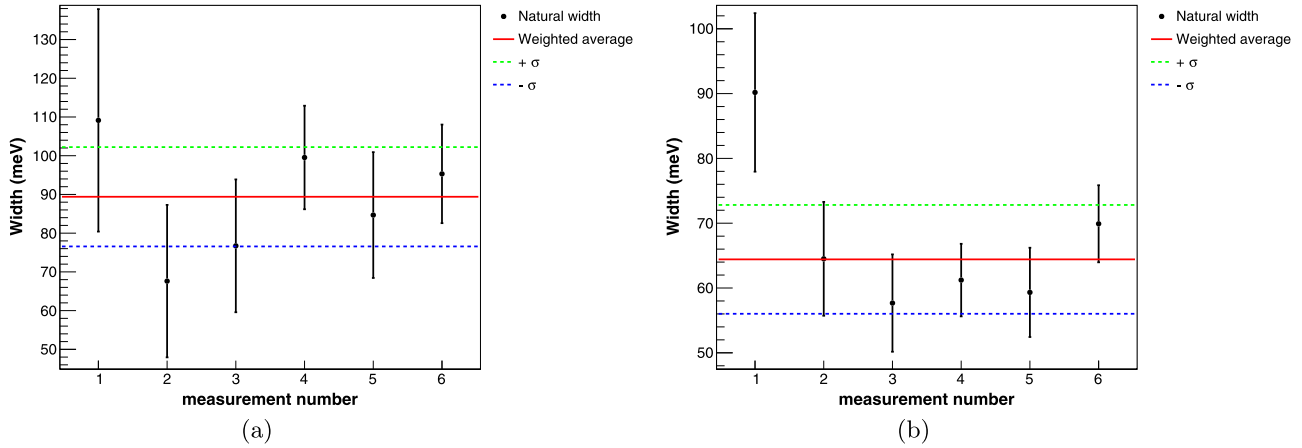
FIG. 4. Natural widths of all spectra recorded during the measurement of the (a) $1s2s2p\,^2P_{1/2} \rightarrow 1s^22s\,^2S_{1/2}$ and (b) $1s2s2p\,^2P_{3/2} \rightarrow 1s^22s\,^2S_{1/2}$ Li-like argon transitions. The weighted average and the 68% confidence interval ($\pm 1\sigma$) are also shown.
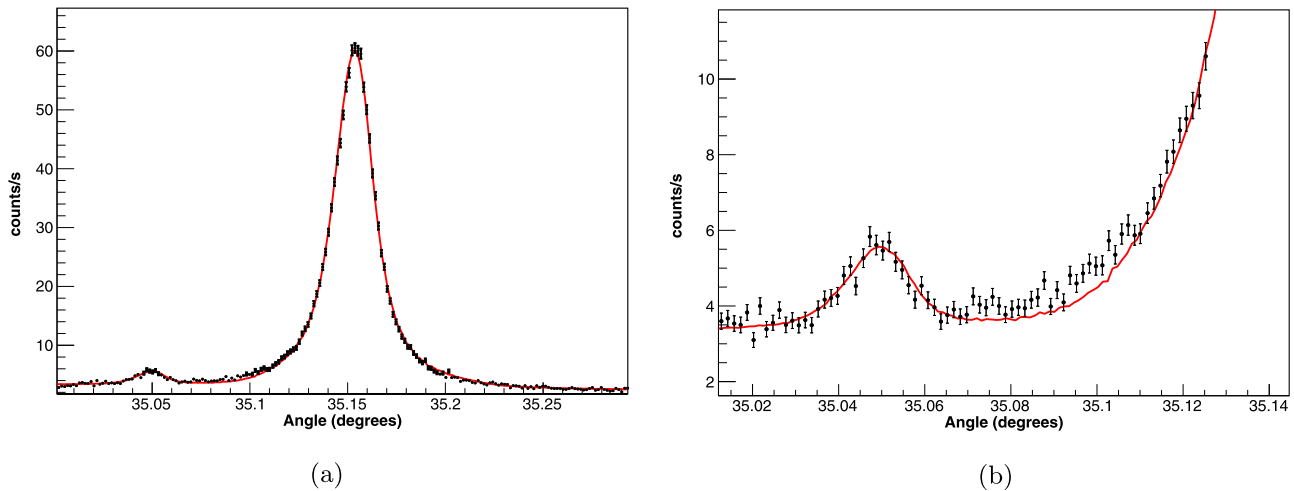
FIG. 5. (a) Spectrum of the $1s2s2p\,^4P_{5/2} \rightarrow 1s^22s\,^2S_{1/2}$ and $1s2s^22p\,^1P_1 \rightarrow 1s^22s^2\,^1S_0$ transitions in Li-like and Be-like sulfur. The best fit corresponds to a Lorentzian width of 0 meV for the $1s2s2p\,^4P_{5/2} \rightarrow 1s^22s\,^2S_{1/2}$ transition. (b) Close-up of the $1s2s2p\,^4P_{5/2} \rightarrow 1s^22s\,^2S_{1/2}$ transition. See the text and Ref. [18] for more details.
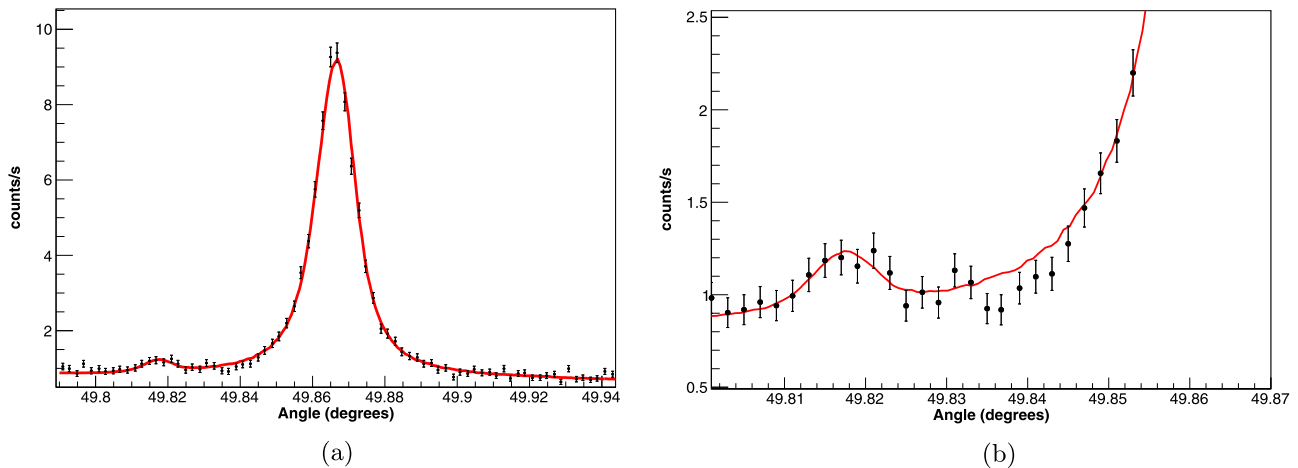
FIG. 6. (a) Spectrum of the $1s2s2p\,^4P_{5/2} \rightarrow 1s^22s\,^2S_{1/2}$ and $1s2s^22p\,^1P_1 \rightarrow 1s^22s^2\,^1S_0$ transitions in Li-like and Be-like argon. The best fit corresponds to a Lorentzian width of 0 meV for the $1s2s2p\,^4P_{5/2} \rightarrow 1s^22s\,^2S_{1/2}$ transition. (b) Close-up of the $1s2s2p\,^4P_{5/2} \rightarrow 1s^22s\,^2S_{1/2}$ transition. See the text and Ref. [18] for more details.
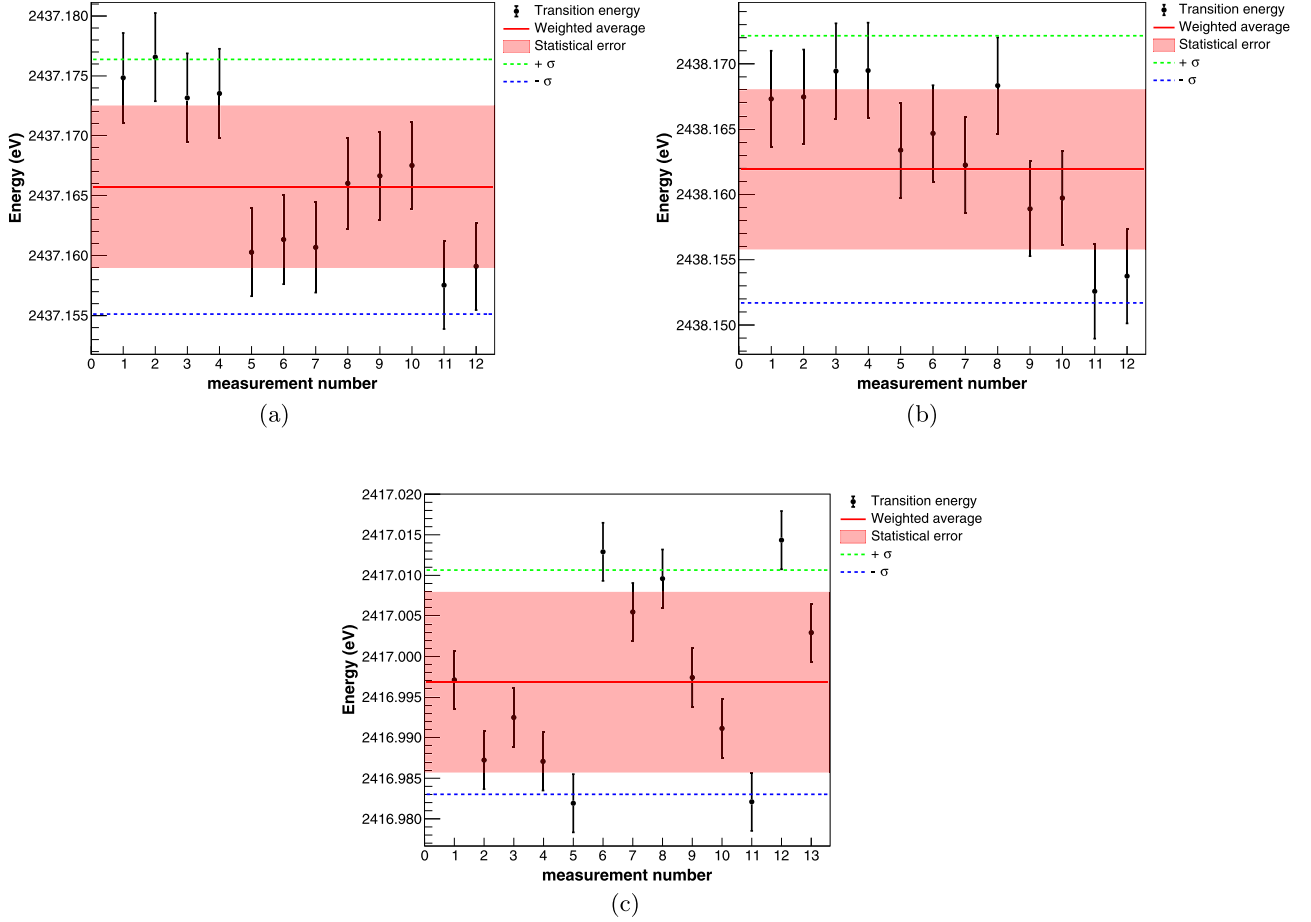
FIG. 7. Li-like sulfur $1s2s2p\,^2P_J \rightarrow 1s^22s\,^2S_{1/2}$ doublet, for (a) $J = 1/2$ and (b) $J = 3/2$, and (c) $1s2s2p\,^4P_{5/2} \rightarrow 1s^22s\,^2S_{1/2}\,M2$ transition energy values from the different pairs of dispersive and nondispersive spectra recorded during the experiment. Error bars correspond to statistical uncertainty obtained from Eq. (3) in the Supplemental Material [63], quadratically combined with the uncertainties in the temperature and angle measurements. The red solid curve corresponds to the weighted average, obtained considering only the statistical uncertainty in each point. The pink shaded area corresponds to the statistical uncertainty and the blue and green dashed lines ($\pm\sigma$) represent the total uncertainty obtained by the quadratic combination of the statistical uncertainty and all the instrumental contributions. Every pair of points corresponds to one day of data taking.

is the second crystal angle, θ_0^1 and θ_0^2 are the offset angles between the experimental and simulated spectra for each line, a is the background intensity, and b is the background slope. The parameters $I_{\max}^j$, θ_0^j, a, and b are adjusted to minimize $\chi^2(\Gamma_L^1, \Gamma_L^2)$. We do a set of simulations, using five different energies $E_k = E_{\text{theor}} + k\Delta E$, with $\Delta E = 0.01$ eV, $k \in \{-2, -1, 0, 1, 2\}$, and ten different temperatures T_l ranging from $20\,^\circ$C to $30\,^\circ$C for each line. Equation (1) and the different simulations are used to find the best line energy and line intensities. Mode details can be found in Sec. I B of the Supplemental Material [63].

From the two bidimensional fit functions, the experimental line energy E_{Expt}^n for spectrum pair number n is obtained from the relation $\Delta\theta_{\text{Expt-simul}}(E_{\text{Expt}}^n, T_{\text{Expt}}) = 0$, where T_{Expt} indicates the measured average temperature on the second crystal. When all experimental energy values for each pair of dispersive and nondispersive spectra have been obtained, a weighted average is performed and the final value of the energy is obtained with the respective statistical uncertainty. The values obtained for each pair of dispersive and nondispersive spectra for both Li-like lines are presented in Fig. 7

for sulfur and Fig. 8 for argon. The weighted average is represented by the red solid line and the red and blue dashed lines represent $+\sigma$ and $-\sigma$, respectively. The error bar at each point corresponds to the statistical uncertainty of obtaining the energy value from the bidimensional fit function, quadratically combined with the uncertainties due to the temperature and angle measurements. Each pair of points on both plots of Figs. 7 and 8 corresponds to one day of data taking.

The systematic uncertainty is obtained in the same way as described in Refs. [18,19,59]. The resulting values for sulfur are presented in Table I. Several contributions are relatively larger than in argon, due to the increased dispersion at lower energy.

3. Transition energies of the $1s2s2p\,^4P_{5/2} \rightarrow 1s^22s\,^2S_{1/2}$ transition and adjacent lines

Using the method described above, we obtain the energy of the $1s2s2p\,^4P_{5/2} \rightarrow 1s^22s\,^2S_{1/2}$ transition in both sulfur and argon; however, for sulfur we find evidence in the residuals of the presence of a third peak, as shown in Fig. 9. In order to certify its existence and obtain its energy, we use advanced

(a)

(b)

(c)
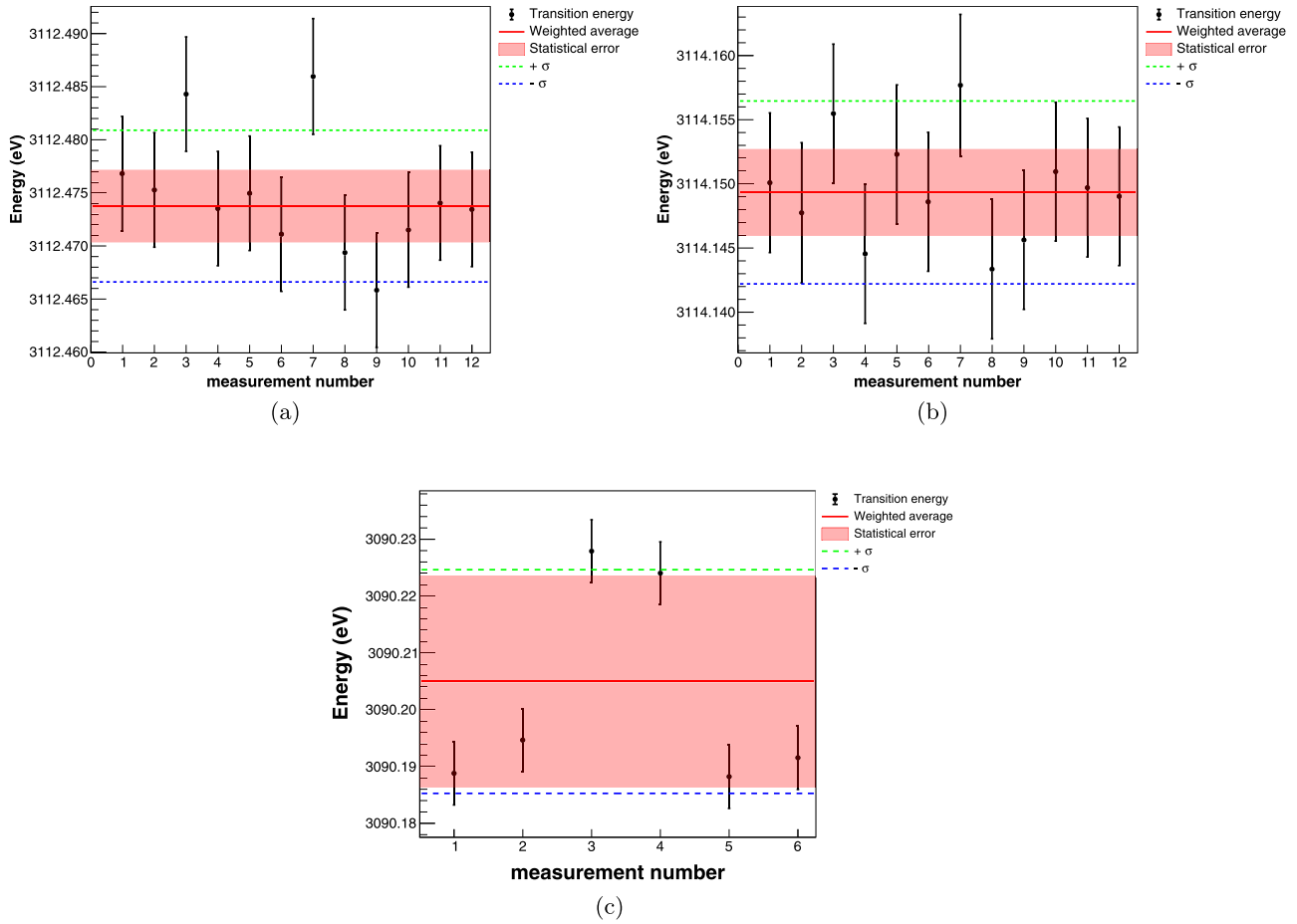
FIG. 8. Li-like argon $1s2s2p\,^2P_J \rightarrow 1s^2 2s\,^2S_{1/2}$ doublet, for (a) $J = 1/2$ and (b) $J = 3/2$, and (c) $1s2s2p\,^4P_{5/2} \rightarrow 1s^2 2s\,^2S_{1/2}$ $M2$ transition energy values for the different pairs of dispersive and nondispersive spectra recorded during the experiment. See the legend of Fig. 7 for details.

Bayesian techniques, as implemented in the NESTEDFIT analysis package described in [65]. This package is based on the methods developed in Refs. [66–69]. We also use the simulated profile for this peak, using the natural width obtained

by first fitting a Voigt profile for the same peak. The shift between the position obtained by the Voigt profile peak and the simulated profile is equal to 1σ. With the Bayesian technique we find statistically significant evidence of the presence

(a)

(b)
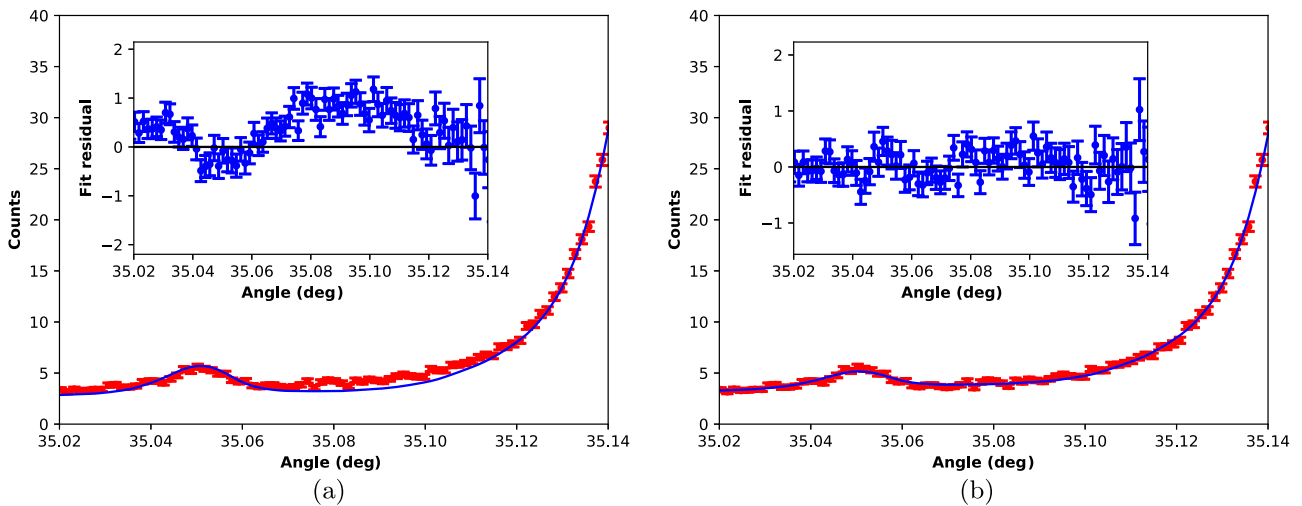
FIG. 9. Close-up of fits to the $1s2s2p\,^4P_{5/2} \rightarrow 1s^2 2s\,^2S_{1/2}$ and $1s2s^2 2p\,^1P_1 \rightarrow 1s^2 2s^2\,^1S_0$ transitions in Li-like and Be-like sulfur (a) without and (b) with inclusion of a third peak. Fitting residuals are shown for each case in the insets. See the text for details.

TABLE I. Contributions to the systematic uncertainties for sulfur. All energies are given in eV.

Contribution	Value (eV)
Index of refraction	0.00055
Angle encoder error (0.2″)	0.00171
Temperature (0.5 °C)	0.00312
Energy-wavelength correction	0.00006
Lattice spacing error	0.00010
Thermal expansion	0.00015
Energy dependence of the width	0.00031
X-ray polarization	0.00513
Variation of x-ray source size (6–12 mm)	0.00462
Crystal tilts (±0.01 °C for each crystal)	0.00085
Vertical divergence (±0.01 mm)	0.00102
Form factors	0.00212
Total	0.00819

of this third peak between the $1s2s2p\,^4P_{5/2} \rightarrow 1s^22s\,^2S_{1/2}$ and $1s2s^22p\,^1P_1 \rightarrow 1s^22s^2\,^1S_0$ transitions. The differences in the fits and residuals when including this peak are shown in Fig. 9. We checked for the possible presence of a fourth peak, but the Bayesian analysis excludes it.

The energy values and error bars of the different daily measurements for this third peak are shown in Fig. 10. Since we use a double-flat-crystal spectrometer, we can be sure that the profile of the lines near this peak, resulting from the simulation, are very accurate since they can be checked with the nondispersive mode spectrum, which does not depend on the shape of the line that is being measured and represents exactly the response function of the instrument. For argon, we do not find statistical evidence of the presence of such a peak. The identification of this peak will be discussed in Sec. IV B.

III. THEORETICAL EVALUATION OF THE ENERGIES AND WIDTHS OF THE MEASURED TRANSITIONS

We have evaluated the energies of the $1s2s2p\,^2P_{1/2} \rightarrow 1s^22s\,^2S_{1/2}$, $1s2s2p\,^2P_{3/2} \rightarrow 1s^22s\,^2S_{1/2}$, and $1s2s2p\,^4P_{5/2} \rightarrow$
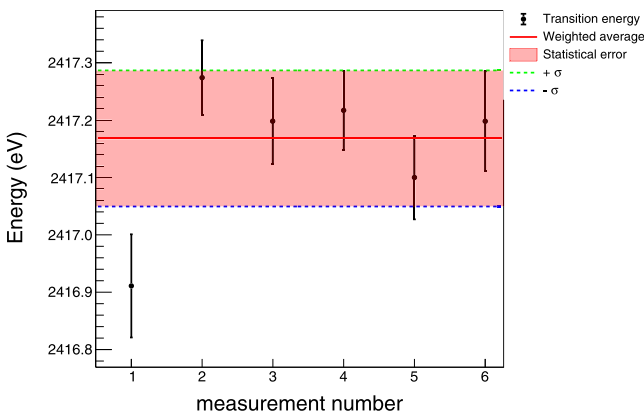

FIG. 10. Energy of the third peak located between the $1s2s2p\,^4P_{5/2} \rightarrow 1s^22s\,^2S_{1/2}$ transition and the $1s2s^22p\,^1P_1 \rightarrow 1s^22s^2\,^1S_0$ one in sulfur. Each point corresponds to the third peak energy as calculated relative to the Li-like $1s2s2p\,^4P_{5/2} \rightarrow 1s^22s\,^2S_{1/2}$ transition energy, for a one day measurement, fitted using Bayesian analysis and an exact profile.

$1s^22s\,^2S_{1/2}$ transitions in sulfur and argon using the code MCDFGME, developed by Desclaux and Indelicato [70–73]. This code has been recently modified to be able to calculate the self-energy screening correction following the model operator approach recently developed in Refs. [74,75], in the same way as our recent work on Be-like argon [19]. We used the 2018 version of the code, which takes into account the most-recent two-loop self-energy correction calculations [76], although their effect is very small here. The full description of the method and the code can be found in Refs. [70,77–79]. The code also evaluates the normal and specific mass shifts, following [80–82], as described in [83,84]. All calculations were done for a finite nucleus modeled as a uniformly charged sphere. The atomic masses were taken from the tables in Ref. [85] and the nuclear radii from [86,87], respectively.

The main advantage of the MCDF approach is the ability to include a large amount of electronic correlation by taking into account a limited number of configurations [88–90]. Here we have included all singly, doubly, and triply excited configurations up to $5g$ orbitals. The calculation is rather difficult for the excited state, when the $1s2s$ core acquires a $^1S_0$ component. In this case, the off-diagonal Lagrange multiplier that is used to maintain the orthogonality between the two orbitals tends to become very small and the $2s$ orbital tends to become identical to the $1s$ one. We thus added the ground-state configuration $1s^22s$ for these cases, which prevents this from occurring.

One-electron radiative corrections are exact QED values. The one-electron self-energy is taken from the work of Mohr and co-workers [91–95] and corrected for finite nuclear size [96]. The self-energy screening and vacuum polarization are calculated following [55,57,71,72,97]. Here we compare the self-energy screening obtained using the Welton approximation [71,72] and the approach from Refs. [74,75]. The two-loop self-energy is taken from [76,98–104]. The SEVP and S(VP)E corrections are obtained from Ref. [102]. The Källèn-Sabry potential is also included, as described in Ref. [105]. We find that for $Z = 16$ and 18, these contributions are smaller than 1 meV. The full Breit interaction and the Uehling potential are included in the self-consistent-field process, which provides higher-order corrections. Projection operators have been included [79] to avoid coupling with the negative-energy continuum. The details of the different contributions for sulfur are presented in Table II and for argon in Table III.

Radiative transition probabilities are evaluated using the method described in Ref. [106]. The orbitals contributing to the wave function are fully relaxed and the resulting nonorthogonality between initial and final wave functions is fully taken into account, following [107,108]. The radiative transition rates to other levels have also been evaluated. We thus take into account, in the total width, all transitions of the type $1s2s2p\,^2P_J \rightarrow 1s^2nl\,j$, with $n \leqslant 7$, $l \leqslant n$, and all possible values of j.

The Auger widths of the $1s2s2p\,^2P_J$ and $1s2s2p\,^4P_{5/2}$ levels are calculated using the MCDFGME code, as described in Ref. [109]: the initial- and final-state orbitals are fully relaxed, we use final-state channel mixing, and we take into account the nonorthogonality between the fully relaxed orbitals in the initial and final states.

TABLE II. Theoretical contributions to the sulfur transition energies, as evaluated with the MCDFGME code. All energies are given in eV. Contributions which are lower than 1 meV are not shown. This includes the Wichmann-Kroll vacuum polarization contribution and two-loop contributions such as two-loop self-energy and mixed self-energy vacuum polarization diagrams (SEVP, S(VP)E) and Källèn-Sabry two-loop vacuum polarization. Higher-order relativistic recoil corrections and higher-order retardation correlation are also too small to be shown.

Contribution	$1s2s2p\,^2P_{1/2} \rightarrow 1s^22s\,^2S_{1/2}$	$1s2s2p\,^2P_{3/2} \rightarrow 1s^22s\,^2S_{1/2}$	$1s2s2p\,^4P_{5/2} \rightarrow 1s^22s\,^2S_{1/2}$
Coulomb+Uehling	2438.584	2439.638	2418.121
Magnetic	−1.423	−1.444	−1.435
Retardation	0.049	0.053	−0.049
Higher-order retardation	0.001	0.001	−0.001
Self-energy	−0.811	−0.808	−0.806
Self-energy screening	0.068	0.070	0.077
Electronic density Uehling	−0.001	−0.001	−0.001
Normal mass shift	−0.042	−0.042	−0.041
Specific mass shift	0.005	0.007	−0.008
Coulomb correlation	0.584	0.542	1.011
Magnetic correlation	0.105	0.104	0.127
Retardation correlation	−0.028	−0.029	−0.030
Total	2437.091	2438.091	2416.964

The results for the radiative and Auger lifetimes and fluorescence yields for sulfur and argon are presented in Tables IV and V, respectively. The transition energies and rates have also been evaluated for comparison with the flexible atomic code (FAC), widely used in plasma physics [110].

IV. RESULTS AND DISCUSSION

A. Values of the widths

The experimental widths obtained using the method explained in Sec. II B 1 are presented for S in Fig. 3 and for Ar in Fig. 4. The values are given in Table VI and compared with theoretical calculations. The comparison is also plotted in Fig. 11.

The comparison shows that for both elements, the $1s2s2p\,^2P_{1/2} \rightarrow 1s^22s\,^2S_{1/2}$ width is larger than that of $1s2s2p\,^2P_{3/2} \rightarrow 1s^22s\,^2S_{1/2}$, by 97% in sulfur and 39% in argon. In contrast, all theoretical predictions give identical

widths for these lines. The agreement between the experimental width of the $1s2s2p\,^2P_{3/2} \rightarrow 1s^22s\,^2S_{1/2}$ transition and theory is good. The width of the $1s2s2p\,^2P_{1/2} \rightarrow 1s^22s\,^2S_{1/2}$ transition, the less intense one, is larger than theory for both elements, an effect most exaggerated for sulfur. The width of the q and r lines has also been measured in iron in Ref. [50]. In that case the two lines were found to have nearly identical widths, in good agreement with theory. A possibility is of course a strong contamination of one of the lines from a satellite transition, which would make it appear broader. A similar problem exists for the intensity ratios. We postpone the discussion about possible contamination to Sec. IV C.

B. Values of the energies

In Figs. 7 and 8 we present the daily energy values measured for the three transitions studied in this work, for sulfur and argon, respectively. These measurements

TABLE III. Theoretical contributions to the argon transition energies, as evaluated with the MCDFGME code. All energies are given in eV. Contributions which are lower than 1 meV are not shown (see Table II caption for details). For argon the Källèn-Sabry contribution starts to be visible.

Contribution	$1s2s2p\,^2P_{1/2} \rightarrow 1s^22s\,^2S_{1/2}$	$1s2s2p\,^2P_{3/2} \rightarrow 1s^22s\,^2S_{1/2}$	$1s2s2p\,^4P_{5/2} \rightarrow 1s^22s\,^2S_{1/2}$
Coulomb+Uehling	3114.855	3116.647	3092.248
Magnetic	−2.023	−2.088	−2.062
Retardation	0.069	0.078	−0.071
Higher-order retardation	0.001	0.001	−0.002
Self-energy	−1.218	−1.213	−1.211
Self-energy screening	0.090	0.095	0.104
Electronic density Uehling	−0.001	−0.001	−0.001
Källèn and Sabry	0.001	0.001	0.001
Normal mass shift	−0.042	−0.042	−0.042
Specific mass shift	0.005	0.007	−0.008
Coulomb correlation	0.579	0.526	0.984
Magnetic correlation	0.128	0.130	0.152
Retardation correlation	−0.033	−0.036	−0.035
Total	3112.411	3114.104	3090.056

TABLE IV. Theoretical sulfur radiative and Auger lifetimes, energies, and fluorescence yields, as evaluated with the MCDFGME code. All En and Mn multipole contributions are included for the radiative transitions. All widths are given in meV and energies in eV.

Final level	$1s2s2p\,^2P_{1/2}$ Width	$1s2s2p\,^2P_{1/2}$ Energy	$1s2s2p\,^2P_{3/2}$ Width	$1s2s2p\,^2P_{3/2}$ Energy	$1s2s2p\,^4P_{5/2}$ Width	$1s2s2p\,^4P_{5/2}$ Energy	Type
$1s^22s\,^2S_{1/2}$	35.08457	2437.090	38.93449	2438.090	7.132×10^{-5}	2416.963	Radiative
All $1s^22pj$	0.00001		0.00001		8.390×10^{-7}		Radiative
All $1s^23lj$	0.01086		0.01305		2.609×10^{-8}		Radiative
All $1s^24lj$	0.00152		0.00189		3.897×10^{-9}		Radiative
All $1s^25lj$	0.00049		0.00062		1.289×10^{-9}		Radiative
All $1s^26lj$	0.00023		0.00029		5.929×10^{-10}		Radiative
All $1s^27lj$	0.00021		0.00016		3.258×10^{-10}		Radiative
Total	0.01330		0.01602		8.712×10^{-7}		Radiative
$1s^2\,^1S_0$	3.1432	1730.106	0.00006	1731.106	5.579×10^{-4}	1709.972	Auger
Total width	38.24107		38.95057		6.300×10^{-4}		
Fluorescence yield	0.917		1.000		0.113		

are averaged, using each pair of dispersive and nondispersive spectrum error bars as weights. These averaged values provide reference-free measurements of the energies of the $1s2s2p\,^2P_J \rightarrow 1s^22s\,^2S_{1/2}$ and $1s2s2p\,^4P_{5/2} \rightarrow 1s^22s\,^2S_{1/2}$ transitions. The energy of the small peak observed between the $1s2s2p\,^4P_{5/2} \rightarrow 1s^22s\,^2S_{1/2}$ and the Be-like diagram line is obtained by using the measured $1s2s2p\,^4P_{5/2} \rightarrow 1s^22s\,^2S_{1/2}$ transition energy as a reference and applying the Bragg law, as the change in shape of the spectrometer response function is negligible for such a small energy difference. We obtain an energy of 2417.17(12) eV, which we compare to all the core-excited $n = 2 \rightarrow n = 1$ transitions we have evaluated with FAC for Li-like, Be-like, and B-like sulfur. We find that only one transition has a significant fluorescence yield (0.97) and an energy very close to our value. It is the $1s2p^2\,^4P_{1/2} \rightarrow 1s^22p\,^2P_{1/2}$ $E1$ transition in lithiumlike sulfur. The theoretical transition energy that we obtained with the FAC is 2417.261 eV and the energy provided in Ref. [32] is 2417.293(16) eV. All Be-like and B-like ions transitions with nearby energies have zero fluorescence yield. There is another Li-like line, corresponding to $1s2p^2\,^4P_{5/2} \rightarrow$

$1s^22p\,^2P_{3/2}$, with an energy of 2417.181(16) eV in Ref. [32] and 2417.132 eV in our FAC calculation, but its fluorescence yield is only 0.17. The same study in Ar did not provide evidence for this line, as the statistics of the spectra are lower.

We provide the experimental energies for the seven transitions studied in this work in Table VII. A detailed comparison with the theoretical values obtained in Sec. III and in other theoretical and experimental works is presented in Table VIII for sulfur and in Table IX for argon. There is generally good agreement between successive experiments and between experiment and the most advanced theoretical calculations from the present work and from Refs. [31,32,115]. However, some older publications, e.g., [112,114,116,117], provide values that differ by approximately 1 eV, because of the lack of proper QED corrections. The more recent work in Ref. [118] gives values that are very far away.

The comparison between the very accurate measurements in Ref. [51], which are measurements relative to the heliumlike $1s2s\,^3S_1 \rightarrow 1s^2\,^1S_0$ $M1$ transition, shows a shift of approximately 0.053 eV in sulfur and approximately 0.025 eV

TABLE V. Theoretical argon radiative and Auger lifetimes, energies, and fluorescence yields, as evaluated with the MCDFGME code. All En and Mn multipole contributions are included for the radiative transitions. All widths are given in meV and energies in eV.

| Final level	$1s2s2p\,^2P_{1/2}$ Width	$1s2s2p\,^2P_{1/2}$ Energy	$1s2s2p\,^2P_{3/2}$ Width	$1s2s2p\,^2P_{3/2}$ Energy	$1s2s2p\,^4P_{5/2}$ Width	$1s2s2p\,^4P_{5/2}$ Energy	Type
$1s^22s\,^2S_{1/2}$	55.98473	3112.410	65.0552	3111.194	1.916×10^{-4}	3114.100	Radiative
All $1s^22pj$	0.00001		0.00002		2.855×10^{-6}		Radiative
All $1s^23lj$	0.01310		0.01703		5.482×10^{-8}		Radiative
All $1s^24lj$	0.00179		0.00246		8.101×10^{-9}		Radiative
All $1s^25lj$	0.00058		0.00081		2.667×10^{-9}		Radiative
All $1s^26lj$	0.00026		0.00038		1.224×10^{-9}		Radiative
All $1s^27lj$	0.00014		0.00021		6.716×10^{-10}		Radiative
Total	0.01588		0.02091		2.922×10^{-6}		Radiative
$1s^2\,^1S_0$	7.1881	2194.053	0.0094	2195.743	9.229×10^{-4}	2171.716	Auger
Total width	63.18875		65.08545		1.117×10^{-3}		
Fluorescence yield	0.886		1.000		0.171		

TABLE VI. Comparison between experimental and theoretical Li-like sulfur and argon $1s2s2p\,^2P_J$, $J = 1/2, 3/2$, and $1s2s2p\,^4P_{5/2}$ level widths. All values are given in meV.

Element	Level	Expt width	Error	Theor. width	Ref.
S	$1s2s2p\,^2P_{1/2} \rightarrow 1s^2 2s\,^2S_{1/2}$	71.6	12.6	38.2	This work (MCDF)
				44.9	This work (FAC)
				42.8	[111]
				42.4	[112]
S	$1s2s2p\,^2P_{3/2} \rightarrow 1s^2 2s\,^2S_{1/2}$	36.3	8.8	38.9	This work (MCDF)
				42.7	This work (FAC)
				41.8	[111]
				41.2	[112]
Ar	$1s2s2p\,^2P_{1/2} \rightarrow 1s^2 2s\,^2S_{1/2}$	89.4	12.8	63.2	This work (MCDF)
				68.4	This work (FAC)
				65.9	[111]
				77.8	[113]
				68.6	[114]
				65.6	[112]
Ar	$1s2s2p\,^2P_{3/2} \rightarrow 1s^2 2s\,^2S_{1/2}$	64.4	8.4	65.1	This work (MCDF)
				68.8	This work (FAC)
				67.7	[111]
				72.2	[113]
				69.7	[114]
				67.4	[112]

in argon, much larger than the combined uncertainties. The reasons for this discrepancy are currently not understood and more investigations are need to clarify the issue.

A comparison between theoretical calculations from Refs. [31,32] and from this work with the present experimental values shows reasonable agreement. For argon, the agreement with Ref. [31] is compatible with the combined error bars. For sulfur, there are larger shifts. The shift with the MCDF calculations of the present work is 3.8 times larger than the experimental uncertainty. It is 2.3 larger when compared to the values from Ref. [32]. The size of these discrepancies is compatible with the expected size of missing theoretical contributions. We can cite higher-order correlation, missing QED corrections to the electron-electron interaction
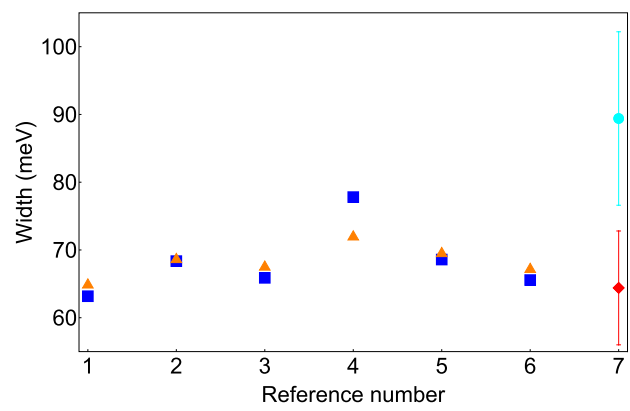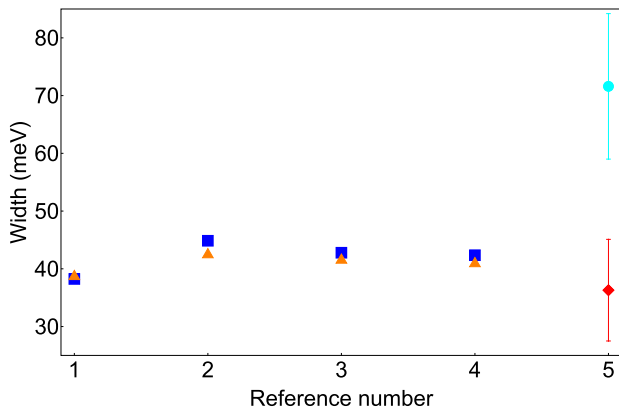
● Experiment (this work) for the 1s 2s 2p $^2P_{1/2} \rightarrow 1s^2 2s\,^2S_{1/2}$ line

■ Theoretical values for the 1s 2s 2p $^2P_{1/2} \rightarrow 1s^2 2s\,^2S_{1/2}$ line

♦ Experiment (this work) for the 1s 2s 2p $^2P_{3/2} \rightarrow 1s^2 2s\,^2S_{1/2}$ line

▲ Theoretical values for the 1s 2s 2p $^2P_{3/2} \rightarrow 1s^2 2s\,^2S_{1/2}$ line

(a)

● Experiment (this work) for the 1s 2s 2p $^2P_{1/2} \rightarrow 1s^2 2s\,^2S_{1/2}$ line

■ Theoretical values for the 1s 2s 2p $^2P_{1/2} \rightarrow 1s^2 2s\,^2S_{1/2}$ line

♦ Experiment (this work) for the 1s 2s 2p $^2P_{3/2} \rightarrow 1s^2 2s\,^2S_{1/2}$ line

▲ Theoretical values for the 1s 2s 2p $^2P_{3/2} \rightarrow 1s^2 2s\,^2S_{1/2}$ line

(b)

FIG. 11. Comparison between the measured and theoretical values for the (a) sulfur and (b) argon doublet widths. The sulfur references are as follows: 1, this work, MCDF; 2, this work, FAC; 3, Ref. [111]; 4, Ref. [112]; and 5, this work, experiment. The argon references are as follows: 1, this work, MCDF; 2, this work, FAC; 3, Ref. [111]; 4, Ref. [113]; 5, Ref. [114]; 6, Ref. [112]; and 7, this work, experiment.

TABLE VII. Experimental values of the energies for the seven lines measured in this work. All energies are given in eV. All energies presented here are reference-free values, except for the $1s2p^{2\,4}P_{1/2} \to 1s^22p\,^2P_{1/2}$ transition in sulfur, which is measured relative to the $1s2s2p\,^4P_{5/2} \to 1s^22s\,^2S_{1/2}$ transition.

Element	Transition	Energy	Statistical uncertainty	Systematic uncertainty	Total uncertainty	ppm
S	$1s2s2p\,^2P_{1/2} \to 1s^22s\,^2S_{1/2}$	2437.1658	0.0068	0.0082	0.011	4.4
S	$1s2s2p\,^2P_{3/2} \to 1s^22s\,^2S_{1/2}$	2438.1619	0.0061	0.0082	0.010	4.2
S	$1s2s2p\,^4P_{5/2} \to 1s^22s\,^2S_{1/2}$	2416.997	0.011	0.0082	0.014	5.7
S	$1s2p^{2\,4}P_{1/2} \to 1s^22p\,^2P_{1/2}$	2417.17[a]	0.12	0.0082	0.12	49
Ar	$1s2s2p\,^2P_{1/2} \to 1s^22s\,^2S_{1/2}$	3112.4737	0.0034	0.0063	0.0071	2.3
Ar	$1s2s2p\,^2P_{3/2} \to 1s^22s\,^2S_{1/2}$	3114.1493	0.0034	0.0063	0.0071	2.3
Ar	$1s2s2p\,^4P_{5/2} \to 1s^22s\,^2S_{1/2}$	3090.205	0.019	0.0063	0.020	6.4

[a]Energy relative to the sulfur $1s2s2p\,^4P_{5/2} \to 1s^22s\,^2S_{1/2}$ transition energy.

(crossed-photon diagrams contributions) or approximate corrections (self-energy screening), and the Auger shift. For example, considering the $1s2s2p\,^2P_{3/2} \to 1s^22s\,^2S_{1/2}$ transition, one finds that the self-energy screening evaluated by the Welton method is 0.067 eV for sulfur and 0.091 eV for argon. If one looks at the same correction evaluated by the effective operator method, one finds 0.070 and 0.095 eV, respectively, i.e., very small changes of 0.003 and 0.004 eV. However, if one uses the self-energy correction to the electron-electron interaction directly evaluated by QED from Ref. [121], one gets 0.091 and 0.122 eV. This corresponds to an increase of the transition energy by 0.024 eV in sulfur and 0.031 eV in argon, i.e., 31% and 48% of the difference between experiment and theory shown in Tables VIII and IX, respectively.

We present in Figs. 12 and 13 a complete comparison between the theoretical calculations in Refs. [31,32,115] and all available experimental results for $10 \leqslant Z \leqslant 28$ for the $1s2s2p\,^2P_J \to 1s^22s\,^2S_{1/2}$, $J = 1/2, 3/2$, transitions. The value from Ref. [53] for the $1s2s2p\,^2P_{3/2} \to 1s^22s\,^2S_{1/2}$, $J = 1/2, 3/2$, transition energy for $Z = 59$ is not plotted as it has a very large error bar and it is the only element measured above $Z = 28$.

TABLE VIII. Comparison between the reference-free measurements from this work (TW) and theoretical and experimental transition energies for lithiumlike sulfur. All energies are given in eV. Here Diff. denotes the energy difference between this work's experimental value and theory; EO denotes the effective operator method.

Experiment			Theory			
Energy	Uncertainty	Ref.	Energy	Uncertainty	Diff.	Ref.
			$1s2s2p\,^2P_{1/2} \to 1s^22s\,^2S_{1/2}$ transition			
2437.166	0.011	TW	2437.087		0.079	TW (Welton)
2437.115	0.005	[51]	2437.090		0.076	TW (EO)
2437.71	0.24	[37]	2437.056		0.110	TW (FAC)
			2437.1		0.066	[111]
			2437.074	0.019	0.092	[32]
			2437.51		−0.349	[112]
			2437.20		−0.037	[119]
			$1s2s2p\,^2P_{3/2} \to 1s^22s\,^2S_{1/2}$ transition			
2438.162	0.010	TW	2438.087		0.075	TW (Welton)
2438.106	0.003	[37]	2438.090		0.072	TW (EO)
			2438.065		0.097	TW (FAC)
			2438.066	0.019	0.096	[32]
			2438.0		0.162	[111]
			2438.17		−0.005	[119]
			2438.47		−0.312	[112]
			$1s2s2p\,^4P_{5/2} \to 1s^22s\,^2S_{1/2}$ transition			
2416.997	0.014	TW	2416.959		0.038	TW (Welton)
			2416.963		0.034	TW (EO)
			2416.286		0.711	TW (FAC)
			2417.162		−0.166	[119]
			2416.963	0.019	−0.034	[32]

TABLE IX. Comparison between the reference-free measurements from this work and theoretical and experimental transition energies for lithiumlike argon. All energies are given in eV. Here Diff. denotes the energy difference between this work's experimental value and theory; EO denotes the effective operator method.

Experiment			Theory			
Energy	Uncertainty	Ref.	Energy	Uncertainty	Diff.	Ref.
$1s2s2p\,^2P_{1/2} \to 1s^2 2s\,^2S_{1/2}$ transition						
3112.4737	0.0071	TW	3112.409		0.065	TW (Welton)
3112.4510	0.0020	[51]	3112.410		0.064	TW (EO)
3112.63	0.16	[37]	3112.360		0.113	TW (FAC)
3112.4203	0.0859	[47]	3112.40		0.074	[111]
3112.405	0.078	[46]	3112.471	0.012	0.003	[31]
3111.795	0.305	[49]	3113.07		−0.595	[112]
			3112.29		0.184	[120]
			3114.70		−2.226	[116]
			3111.19		1.280	[117]
			3110.74		1.732	[114]
			3112.60		−0.127	[119]
			3118.04		−5.562	[118]
			3112.40		0.074	[113]
$1s2s2p\,^2P_{3/2} \to 1s^2 2s\,^2S_{1/2}$ transition						
3114.1493	0.0071	TW	3114.098		0.051	TW (Welton)
3114.1220	0.0020	[51]	3114.103		0.046	TW (EO)
3114.190	0.078	[37]	3114.061		0.088	TW (FAC)
3114.132	0.078	[46]	3114.1417	0.0055	0.008	[31]
3114.078	0.086	[47]	3114.10		0.049	[111]
3113.97	0.12	[49]	3114.22		−0.075	[119]
			3114.71		−0.562	[112]
			3114.01		0.139	[120]
			3116.40		−2.251	[116]
			3113.07		1.080	[117]
			3112.44		1.713	[114]
			3119.69		−5.540	[118]
			3114.15		−0.001	[113]
$1s2s2p\,^4P_{5/2} \to 1s^2 2s\,^2S_{1/2}$ transition						
3090.205	0.020	TW	3090.050		0.155	TW (Welton)
3090.25	0.12	[47]	3090.055		0.150	TW (EO)
3091.0	2.0	[54]	3089.374		0.831	TW (FAC)
			3090.32		−0.114	[119]
			3089.31		0.895	[120]
			3090.10		0.105	[116]
			3090.1456	0.0046	0.059	[31]

C. Values for the intensity ratios of the $1s2s2p\,^2P_J$ doublet

In addition to the measurement of the natural width and energy of each transition in the $1s2s2p\,^2P_J$ lines in sulfur and argon, we have been able to obtain the ratio between the intensities of the two components of the doublet. This intensity ratio provides an experimental measurement of the relative fluorescence yields of the two transitions.

We have performed two high statistics simulations (one for each line), with the natural widths and energies of the two transitions obtained in this analysis, to fit the spectra with the function from Eq. (1). From the fit to the experimental dispersive spectrum, the optimized adjustable coefficients of the fit function were obtained from a χ^2 minimization. With the coefficients provided in this procedure, the integral of each individual peak I_1 and I_2 has been numerically obtained

from

$$I_1 = \int_{\theta_i}^{\theta_f} I_{\max}^1 S_{E_{\mathrm{Expt}}, \Gamma_L^{\mathrm{Expt}}, \Gamma_G^{\mathrm{Expt}}, T_{\mathrm{Expt}}}^1 (\theta - \theta_0^1)\, d\theta,$$

$$I_2 = \int_{\theta_i}^{\theta_f} I_{\max}^2 S_{E_{\mathrm{Expt}}, \Gamma_L^{\mathrm{Expt}}, \Gamma_G^{\mathrm{Expt}}, T_{\mathrm{Expt}}}^2 (\theta - \theta_0^2)\, d\theta, \quad (2)$$

where θ_i and θ_f are the angular range of the experimental dispersive spectrum and S^1 and S^2 the interpolated simulated dispersive spectra of each transition performed with the experimental energy (E_{Expt}) and natural width (Γ_L^{Expt}) and the Gaussian width from Ref. [18]. As a check, the numerical integration of the total fit function from Eq. (1) to the spectrum, with its background removed, has also been performed and its result compared with the sum of the individual
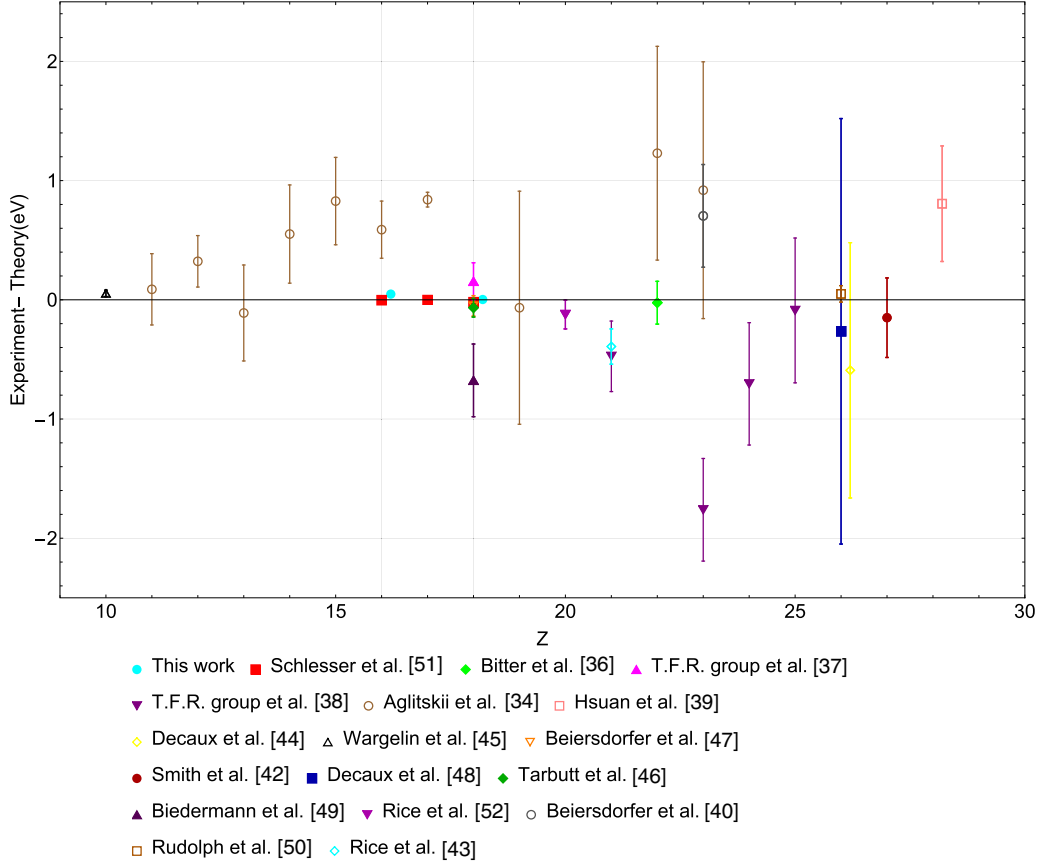
FIG. 12. Comparison between theory [31,32,115] and experiment for the $1s2s2p\,^2P_{1/2} \to 1s^2 2s\,^2S_{1/2}$ transition. Experimental values are from Schlesser *et al.* [51], Bitter *et al.* [36], TFR group *et al.* [37], TFR group *et al.* [38], Aglitskii *et al.* [34], Hsuan *et al.* [39], Decaux *et al.* [44], Wargelin *et al.* [45], Beiersdorfer *et al.* [47], Smith *et al.* [42], Decaux *et al.* [48], Tarbutt *et al.* [46], Biedermann *et al.* [49], Rice *et al.* [52], Beiersdorfer *et al.* [40], Rudolph *et al.* [50], and Rice *et al.* [43].

integrals of Eq. (2). The numerical integrals have been calculated with the data analysis framework ROOT from CERN [122–124] through the MATHMORE library. This library uses the integration algorithms of GNU Scientific Library [125], which reimplements the algorithms used in the QUADPACK [126], a numerical integration package written in FORTRAN. As an example, we find for the sulfur spectrum in Fig. 1 a total area of 0.4116(64), while the area under the $1s2s2p\,^2P_{1/2} \to 1s^2 2s\,^2S_{1/2}$ line is 0.1592(64) and the area under the $1s2s2p\,^2P_{3/2} \to 1s^2 2s\,^2S_{1/2}$ is 0.2525(67). For the argon spectrum in Fig. 2, we find 0.1227(29), 0.0328(29), and 0.0900(30), respectively.

The integration of each peak area has been performed for all dispersive spectra. The ratios between the intensities of the $1s2s2p\,^2P_{1/2} \to 1s^2 2s\,^2S_{1/2}$ and $1s2s2p\,^2P_{3/2} \to 1s^2 2s\,^2S_{1/2}$ transitions are presented in Figs. 14 and 15 for all recorded dispersive spectra of sulfur and argon, respectively. The weighted average is represented by the red solid line and the $\pm\sigma$ values are represented by the green and blue dashed lines. The ratios between the two transitions are 0.603(21) for sulfur and 0.358(13) for argon. However, as discussed in [127], the number of x rays from a given transition that reach the detector in a DCS depends not only on the balance between the feeding mechanisms and the radiative transition intensity, but also on the geometrical settings, on the shape of the collimator, and on the angular acceptance of the first

Bragg crystal. The transmission functions for the energy range 2430–2445 eV in sulfur and 3085–3125 eV in argon are presented in Fig. 16. Because the dispersion is much higher for sulfur and the absorption in the crystal is higher, the curve for sulfur is asymmetric. The curve for sulfur was thus fitted with splines to obtain a transmission value for the $1s2s2p\,^2P_{1/2} \to 1s^2 2s\,^2S_{1/2}$ and $1s2s2p\,^2P_{3/2} \to 1s^2 2s\,^2S_{1/2}$ lines. One gets the spectrometer correction to the line intensities

$$\frac{I_{E_{J=1/2}}}{I_{E_{J=3/2}}} = 1.0399 \tag{3}$$

by inserting the experimental values of the line energies from Table VIII into the spline fit. Applying this correction to the value shown in Fig. 14, we obtain a ratio of 0.627(22) for the relative intensities of the two lines in Li-like sulfur.

For argon, we were able to fit the symmetric curve and found the normalized hyperbolic expression [127]

$$I(E) = 1.048\,15 - 6.276\,47 \times 10^{-5}$$
$$\times \sqrt{|588\,509 + 690\,026(E - 3103.89)^2|}. \tag{4}$$

Entering the line energies in Eq. (4), we obtain the correction

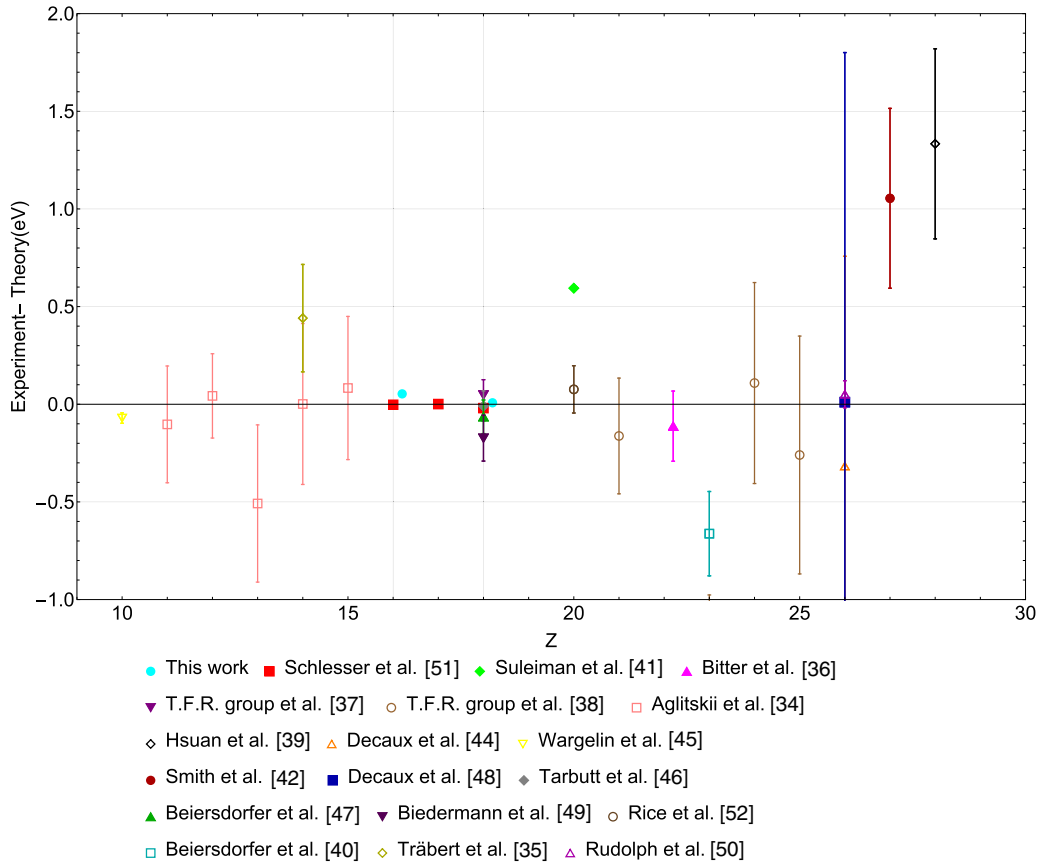$$\frac{I_{E_{J=1/2}}}{I_{E_{J=3/2}}} = 1.1091, \tag{5}$$

FIG. 13. Comparison between theory [31,32,115] and all available experiment for the $1s2s2p\,^2P_{3/2} \rightarrow 1s^2 2s\,^2 S_{1/2}$ transition. Experimental values are from Schlesser *et al.* [51], Suleiman *et al.* [41], Bitter *et al.* [36], TFR Group *et al.* [37], TFR Group *et al.* [38], Aglitskii *et al.* [34], Hsuan *et al.* [39], Decaux *et al.* [44], Wargelin *et al.* [45], Smith *et al.* [42], Decaux *et al.* [48], Tarbutt *et al.* [46], Beiersdorfer *et al.* [47], Biedermann *et al.* [49], Rice *et al.* [52], Beiersdorfer *et al.* [40], Träbert *et al.* [35], Rudolph *et al.* [50], and Rice *et al.* [43].

which, multiplied by the ratio between the peak intensities given in Fig. 15, gives the final value of 0.397(14).

Assuming a statistical population of the levels, the fluorescence yield of Tables IV and V leads to an intensity ratio of
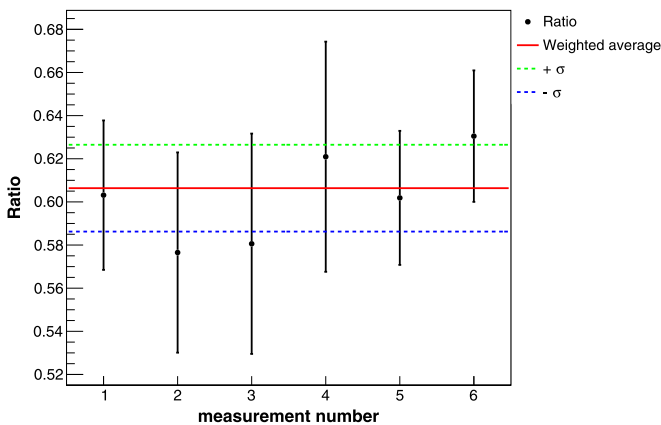

FIG. 14. Ratio between the $1s2s2p\,^2P_{1/2} \rightarrow 1s^2 2s\,^2 S_{1/2}$ and $1s2s2p\,^2P_{3/2} \rightarrow 1s^2 2s\,^2 S_{1/2}$ transition intensities for all recorded dispersive spectra in sulfur. The weighted average value of 0.603 is represented by the red solid line and the $\pm\sigma = 0.021$ are represented by the green and blue dashed lines. The error bar at each point corresponds to the contribution of the uncertainty from the numerical integration of each peak.
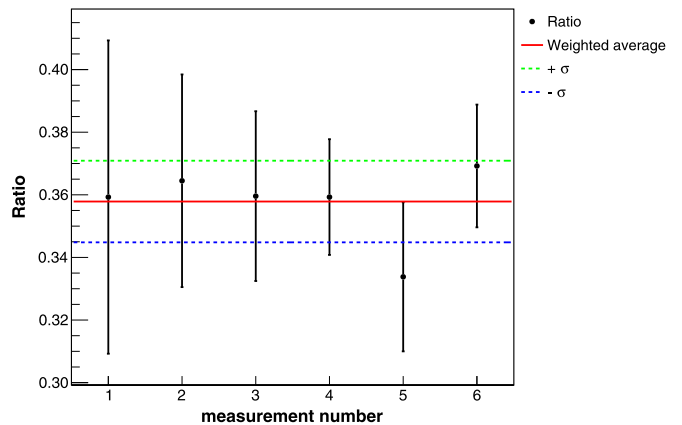

FIG. 15. Ratio between the $1s2s2p\,^2P_{1/2} \rightarrow 1s^2 2s\,^2 S_{1/2}$ and $1s2s2p\,^2P_{3/2} \rightarrow 1s^2 2s\,^2 S_{1/2}$ transition intensities for all recorded dispersive spectra in argon. The weighted average value of 0.358 is represented by the red solid line and the $\pm\sigma = 0.013$ are represented by the green and blue dashed lines. The error bar at each point corresponds to the contribution of the uncertainty from the numerical integration of each peak.
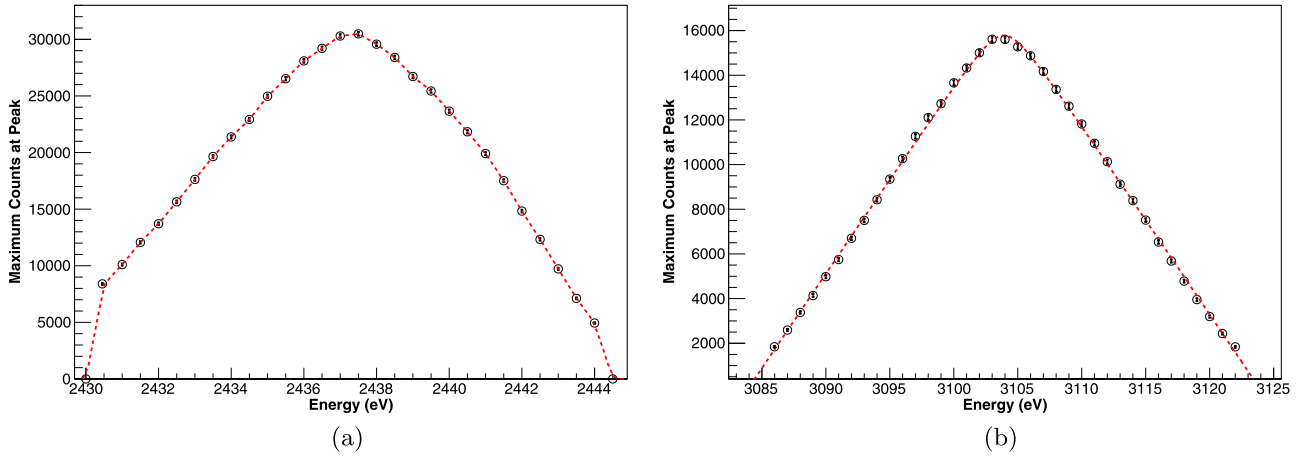
FIG. 16. Transmitted intensity by the spectrometer for Li-like (a) sulfur and (b) argon as a function of x-ray energy following [127]. The red curve represents a fit with splines in sulfur and the fit with Eq. (4) in argon.

0.46 for sulfur and 0.44 for argon. This is consistent with the experimental value for argon, but not for sulfur.

To understand this difference, we have investigated possible line blends, as presented in Fig. 17 for sulfur and Fig. 18 for argon. We considered at the same time other Li-like lines, as well as Be-like and B-like ones. For Li-like lines we used transition energies from Refs. [31,32]. The relative intensities have been obtained using the FAC and evaluating all possible radiative and Auger transitions for a given initial level. For

argon, these calculations are in good agreement with the results from Ref. [113].

For sulfur (Fig. 17) the $1s2p^2\,^2P_{3/2} \rightarrow 1s^22p\,^2P_{1/2}$ transition is blended with the lower-energy member of the observed doublet, the $1s2s2p\,^2P_{1/2} \rightarrow 1s^22s\,^2S_{1/2}$ transition, with a difference of energy of only 0.07 eV. However, this line has a relative intensity of only 7.53%. The other intense line, originating from the same level as the $1s2p^2\,^2P_{3/2} \rightarrow 1s^22p\,^2P_{3/2}$ line, has a relative intensity of 85.4%, but it lies outside the
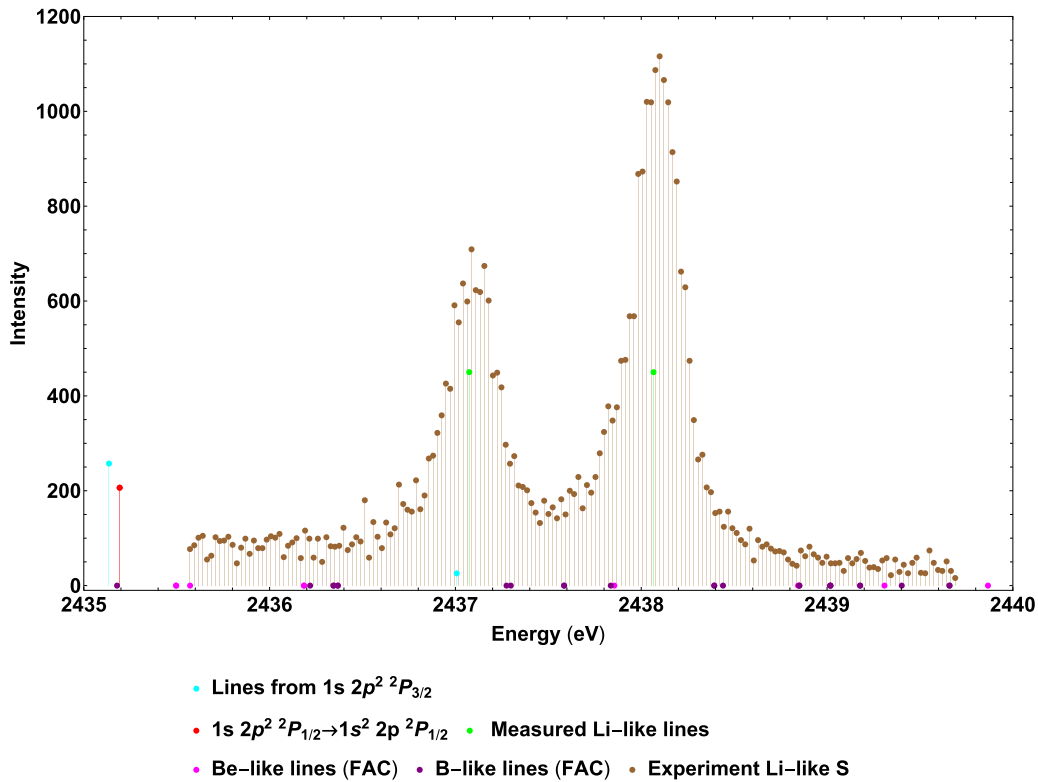

FIG. 17. Possible blends to the $1s2s2p\,^2P_{1/2} \rightarrow 1s^22s\,^2S_{1/2}$ and $1s2s2p\,^2P_{3/2} \rightarrow 1s^22s\,^2S_{1/2}$ transitions in sulfur. The $1s2p^2\,^2P_{3/2} \rightarrow 1s^22p\,^2P_{3/2}$, $1s2p^2\,^2P_{3/2} \rightarrow 1s^22p\,^2P_{1/2}$, and $1s2p^2\,^2P_{1/2} \rightarrow 1s^22p\,^2P_{1/2}$ transition energies are from Ref. [32]. The relative intensities of the $1s2p^2\,^2P_{3/2} \rightarrow 1s^22p\,^2P_{3/2}$ and $1s2p^2\,^2P_{3/2} \rightarrow 1s^22p\,^2P_{1/2}$ transitions are evaluated using branching ratios calculated with the FAC. The intensity of the $1s2p^2\,^2P_{1/2} \rightarrow 1s^22p\,^2P_{1/2}$ transition is arbitrary, but it is the most intense of the doublet. The energies and relative intensities of the Be-like and B-like lines are evaluated using the FAC. Their contributions are very small.
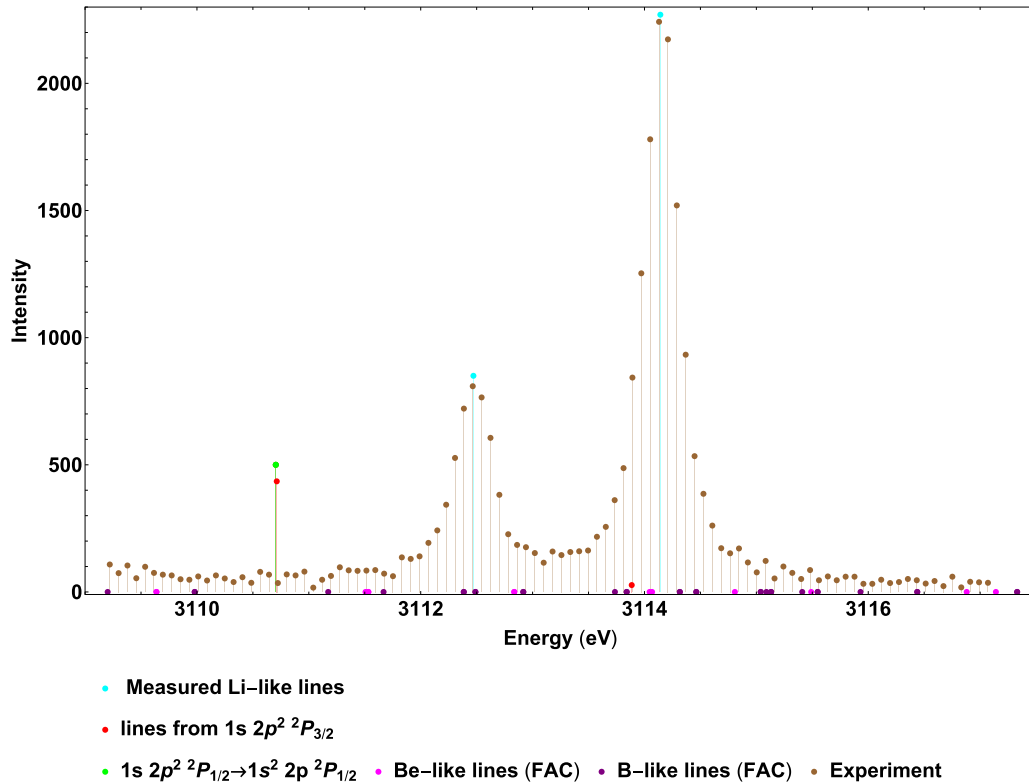
FIG. 18. Possible blends to the $1s2s2p\,^2P_{1/2} \rightarrow 1s^2 2s\,^2S_{1/2}$ and $1s2s2p\,^2P_{3/2} \rightarrow 1s^2 2s\,^2S_{1/2}$ transitions in argon. The $1s2p^2\,^2P_{3/2} \rightarrow 1s^2 2p\,^2P_{3/2}$, $1s2p^2\,^2P_{3/2} \rightarrow 1s^2 2p\,^2P_{1/2}$, and $1s2p^2\,^2P_{1/2} \rightarrow 1s^2 2p\,^2P_{1/2}$ transition energies are from Ref. [31]. The relative intensities of the $1s2p^2\,^2P_{3/2} \rightarrow 1s^2 2p\,^2P_{3/2}$ and $1s2p^2\,^2P_{3/2} \rightarrow 1s^2 2p\,^2P_{1/2}$ transitions are evaluated using branching ratios calculated with the FAC. The absence of a line at the expected position in the experimental spectrum shows that the contribution of this line to the intensity of the $1s2s2p\,^2P_J \rightarrow 1s^2 2s\,^2S_{1/2}$ doublet is negligible. The energies and relative intensities of the Be-like and B-like lines are also evaluated using the FAC. Their contributions are very small.

window of energy scanned during the experiment. However, this line is not observed in argon, while it is in the scanned area (see Fig. 18). It is thus highly unlikely, with two elements so close in Z, that the contamination would be more significant in sulfur than in argon. Figure 17 shows that no Be-like and B-like core-excited transitions have a relative intensity able to explain the difference between S and Ar.

In argon, as seen in Fig. 18, the higher-energy component of the doublet, the $1s2s2p\,^2P_{3/2} \rightarrow 1s^2 2s\,^2S_{1/2}$ transition, is blended with the $1s2p^2\,^2P_{3/2} \rightarrow 1s^2 2p\,^2P_{1/2}$ transition (the energy difference is 0.26 eV). However, it has a relative intensity of only 5.4%, while the other intense line originating from the same level, the $1s2p^2\,^2P_{3/2} \rightarrow 1s^2 2p\,^2P_{3/2}$ one, has a relative intensity of 87%. Since no line is seen at the expected position, we conclude that this blend cannot explain the difference. The figure also shows that, as observed in sulfur, no Be-like or B-like line can change the relative intensity of the $1s2s2p\,^2P_J \rightarrow 1s^2 2s\,^2S_{1/2}$ doublet.

Both sulfur and argon lithiumlike doublets were also tested for the presence of a third contaminant peak, using the method described in Sec. II B 3. Bayesian evidence was evaluated for two models: (i) the two simulated response functions superimposed on a linear background, as used in the aforementioned analysis, and (ii) the two simulated response functions superimposed on a linear background and a third

Voigt peak. The Doppler broadening of the Voigt peak was fixed to 90 meV, consistent with the broadening of the S He-like $M1$ peak, while the Lorentzian width was left free and the centroid allowed to be anywhere in the spectrum. The Bayesian evidence was significantly higher when a third peak was added with a gain in logarithm of the Bayesian evidence of 60.62(8) and 10.55(9) for the lithiumlike S and Ar doublets, respectively. The corresponding p value are approximately 2.63×10^{-29} and 2.78×10^{-7}, respectively. However, in both cases the ratio of intensities between the third peak and the $1s2s2p\,^2P_{1/2} \rightarrow 1s^2 2s\,^2S_{1/2}$ transition was found to be less than 1% and the centroid of the third peak far to the left of the line, thus unable to explain the intensity discrepancy seen in the data.

We indeed also tested the different spectra for possible contamination by lines from other elements. We first used the NIST line database [128] to check for possible lines from other ions in the plasma. For sulfur, we found lines of Si, W, Ga, Sr, Cu, and Kr in the energy range. Yet only the $1s^2 2s^2 2p^4 4d$, $J = 5/2 \rightarrow 1s^2 2s^2 2p^5$, $J = 3/2$ transition in F-like Kr is close enough to be a possible contaminant. Its energy has been measured in Ref. [129] and is 2438.72 eV, too far in the tail of the $1s2s2p\,^2P_{3/2} \rightarrow 1s^2 2s\,^2S_{1/2}$ peak (0.55 eV) to have an effect. Moreover, since we inject only SF_6 and oxygen, we have no krypton contamination. This

was verified using the quadrupole mass spectrometer, which monitors continuously the composition of the gas in the ECRIS.

For argon, a similar analysis shows that there are some lines from Mo, W, and Kr, which have energies in the range where the lines of interest are measured, but no close coincidence could be found. We then checked for the possibility of x rays emitted by solid elements composing the instrument, using Ref. [58]. The only possible coincidence would be due to the L_2M1 line at 3112.58(10) eV in indium, which coincides with the energy of the $1s2p^2\,^2P_{1/2} \rightarrow 1s^22p\,^2P_{1/2}$ transition in Ar, but there is no indium in our apparatus.

We can now return to the difference in widths between the two components of the $1s2s2p\,^2P_J \rightarrow 1s^22s\,^2S_{1/2}$ doublet discussed in Sec. IV A. The absence of contamination discussed above shows that the difference in width observed between the two lines of the doublet cannot be explained by the presence of other unresolved lines.

V. CONCLUSION

We have made a reference-free measurement of the two allowed $1s2s2p\,^2P_{3/2} \rightarrow 1s^22s\,^2S_{1/2}$ and $1s2s2p\,^2P_{1/2} \rightarrow 1s^22s\,^2S_{1/2}$ transitions and the forbidden $1s2s2p\,^4P_{5/2} \rightarrow 1s^22s\,^2S_{1/2}$ $M2$ transition in core-excited lithiumlike sulfur and argon. Our results have accuracies comparable to those of the best-available relative measurements [51]. Previously, the $M2$ transition was known only in argon, with a 3-times-larger uncertainty. We also measured the energy of the $1s2p^2\,^4P_{1/2} \rightarrow 1s^22p\,^2P_{1/2}$ transition in Li-like sulfur, relative to the $1s2s2p\,^4P_{5/2} \rightarrow 1s^22s\,^2S_{1/2}$ transition. We have measured the widths and the intensity ratios of the $1s2s2p\,^2P_{3/2} \rightarrow 1s^22s\,^2S_{1/2}$ and $1s2s2p\,^2P_{1/2} \rightarrow 1s^22s\,^2S_{1/2}$ line doublet. The agreement between our experimental energies and the most-comprehensive state-of-the-art theoretical values (this work and [31]) is within the combined error bars for argon. It is not as good for sulfur (Ref. [32] and this work). The differences are probably due to the missing correlation contributions, larger at lower Z, to missing QED corrections, and to Auger shifts. More high-accuracy measurements of these transitions for other elements are required to better understand the reasons for the discrepancy between experiment and theory.

The width of the $1s2s2p\,^2P_{3/2} \rightarrow 1s^22s\,^2S_{1/2}$ transition agrees with theory for both sulfur and argon, while the width of the $1s2s2p\,^2P_{1/2} \rightarrow 1s^22s\,^2S_{1/2}$ transition disagrees. This width discrepancy is not observed in iron [50]. We have been able to exclude contaminations by other lines as a cause for this discrepancy. Moreover, the $1s2s2p\,^2P_J \rightarrow 1s^22s\,^2S_{1/2}$ transition intensity ratios do not agree with theory. Here it is important to note that such a discrepancy in line intensity ratio as we have observed in sulfur has been observed in the past. For example, it has been observed in very clean conditions in Ne-like iron, between the $2p^5_{1/2}3d_{3/2},\ J = 1 \rightarrow 2p^6,\ J = 0$ and the $2p^5_{1/2}3d_{5/2},\ J = 1 \rightarrow 2p^6,\ J = 0$ lines, for which the predicted ratio is 40% larger than measured [130]. Measurement of these transitions in other elements such as chlorine and with $Z > 18$ to have a better idea of the evolution of the widths and intensity ratios as a function of Z is left for future work.

[1] P. Indelicato, J. Phys. B **52**, 232001 (2019).

[2] C. G. Parthey, A. Matveev, J. Alnis, B. Bernhardt, A. Beyer, R. Holzwarth, A. Maistrou, R. Pohl, K. Predehl, T. Udem *et al.*, Phys. Rev. Lett. **107**, 203001 (2011).

[3] A. Beyer, L. Maisenbacher, A. Matveev, R. Pohl, K. Khabarova, A. Grinin, T. Lamour, D. C. Yost, T. W. Hänsch, N. Kolachevsky *et al.*, Science **358**, 79 (2017).

[4] H. Fleurbaey, S. Galtier, S. Thomas, M. Bonnaud, L. Julien, F. Biraben, F. Nez, M. Abgrall, and J. Guéna, Phys. Rev. Lett. **120**, 183001 (2018).

[5] H. Häffner, T. Beier, N. Hermanspahn, H.-J. Kluge, W. Quint, S. Stahl, J. Verdú, and G. Werth, Phys. Rev. Lett. **85**, 5308 (2000).

[6] S. Sturm, F. Kohler, J. Zatorski, A. Wagner, Z. Harman, G. Werth, W. Quint, C. H. Keitel, and K. Blaum, Nature (London) **506**, 467 (2014).

[7] F. Köhler, S. Sturm, A. Kracke, G. Werth, W. Quint, and K. Blaum, J. Phys. B **48**, 144032 (2015).

[8] J. Zatorski, B. Sikora, S. G. Karshenboim, S. Sturm, F. Köhler-Langes, K. Blaum, C. H. Keitel, and Z. Harman, Phys. Rev. A **96**, 012502 (2017).

[9] J. Verdú, S. Djekić, S. Stahl, T. Valenzuela, M. Vogel, G. Werth, T. Beier, H.-J. Kluge, and W. Quint, Phys. Rev. Lett. **92**, 093002 (2004).

[10] S. Sturm, A. Wagner, B. Schabinger, J. Zatorski, Z. Harman, W. Quint, G. Werth, C. H. Keitel, and K. Blaum, Phys. Rev. Lett. **107**, 023002 (2011).

[11] S. Sturm, A. Wagner, M. Kretzschmar, W. Quint, G. Werth, and K. Blaum, Phys. Rev. A **87**, 030501(R) (2013).

[12] A. Wagner, S. Sturm, F. Köhler, D. A. Glazov, A. V. Volotka, G. Plunien, W. Quint, G. Werth, V. M. Shabaev, and K. Blaum, Phys. Rev. Lett. **110**, 033003 (2013).

[13] A. Gumberidze, T. Stöhlker, D. Banaś, K. Beckert, P. Beller, H. F. Beyer, F. Bosch, S. Hagmann, C. Kozhuharov, D. Liesen, F. Nolden, X. Ma, P. H. Mokler, M. Steck, D. Sierpowski, and S. Tashenov, Phys. Rev. Lett. **94**, 223001 (2005).

[14] H. Bruhns, J. Braun, K. Kubiček, J. R. C. López-Urrutia, and J. Ullrich, Phys. Rev. Lett. **99**, 113001 (2007).

[15] K. Kubiček, P. H. Mokler, V. Mäckel, J. Ullrich, and J. R. C. López-Urrutia, Phys. Rev. A **90**, 032508 (2014).

[16] V. A. Yerokhin and V. M. Shabaev, J. Phys. Chem. Ref. Data **44**, 033103 (2015).

[17] S. W. Epp, R. Steinbrügge, S. Bernitt, J. K. Rudolph, C. Beilmann, H. Bekker, A. Müller, O. O. Versolato, H.-C. Wille, H. Yavaş, J. Ullrich, and J. R. C. López-Urrutia, Phys. Rev. A **92**, 020502(R) (2015).

[18] P. Amaro, S. Schlesser, M. Guerra, E. O. Le Bigot, J.-M. Isac, P. Travers, J. P. Santos, C. I. Szabo, A. Gumberidze, and P. Indelicato, Phys. Rev. Lett. **109**, 043005 (2012).

[19] J. Machado, C. I. Szabo, J. P. Santos, P. Amaro, M. Guerra, A. Gumberidze, G. Bian, J. M. Isac, and P. Indelicato, Phys. Rev. A **97**, 032517 (2018).

[20] A. N. Artemyev, V. M. Shabaev, V. A. Yerokhin, G. Plunien, and G. Soff, Phys. Rev. A **71**, 062104 (2005).

[21] J. Schweppe, A. Belkacem, L. Blumenfeld, N. Claytor, B. Feinberg, H. Gould, V. E. Kostroun, L. Levy, S. Misawa, J. R. Mowat, and M. H. Prior, Phys. Rev. Lett. **66**, 1434 (1991).

[22] C. Brandau, C. Kozhuharov, A. Müller, W. Shi, S. Schippers, T. Bartsch, S. Böhm, C. Böhme, A. Hoffknecht, H. Knopp *et al.*, Phys. Rev. Lett. **91**, 073202 (2003).

[23] P. Beiersdorfer, H. Chen, D. B. Thorn, and E. Träbert, Phys. Rev. Lett. **95**, 233003 (2005).

[24] P. Beiersdorfer, D. Knapp, R. E. Marrs, S. R. Elliott, and M. H. Chen, Phys. Rev. Lett. **71**, 3939 (1993).

[25] P. Beiersdorfer, A. Osterheld, S. R. Elliott, M. H. Chen, D. Knapp, and K. Reed, Phys. Rev. A **52**, 2693 (1995).

[26] P. Beiersdorfer, A. L. Osterheld, J. H. Scofield, J. R. C. López-Urrutia, and K. Widmann, Phys. Rev. Lett. **80**, 3022 (1998).

[27] X. Zhang, N. Nakamura, C. Chen, M. Andersson, Y. Liu, and S. Ohtani, Phys. Rev. A **78**, 032504 (2008).

[28] Y. Nakano, Y. Takano, T. Ikeda, Y. Kanai, S. Suda, T. Azuma, H. Brauning, A. Brauning-Demian, D. Dauvergne, T. Stohlker, and Y. Yamazaki, Phys. Rev. A **87**, 060501(R) (2013).

[29] Y. S. Kozhedub, A. V. Volotka, A. N. Artemyev, D. A. Glazov, G. Plunien, V. M. Shabaev, I. I. Tupitsyn, and T. Stöhlker, Phys. Rev. A **81**, 042513 (2010).

[30] J. Sapirstein and K. T. Cheng, Phys. Rev. A **83**, 012504 (2011).

[31] V. A. Yerokhin and A. Surzhykov, Phys. Rev. A **86**, 042507 (2012).

[32] V. A. Yerokhin, A. Surzhykov, and A. Müller, Phys. Rev. A **96**, 042505 (2017).

[33] A. H. Gabriel, Mon. Not. R. Astron. Soc. **160**, 99 (1972).

[34] E. V. Aglitskii, V. A. Boiko, S. M. Zakharov, S. A. Pikuz, and A. Y. Faenov, Sov. J. Quantum Electron. **4**, 500 (1974).

[35] E. Träbert, I. Armour, S. Bashkin, N. Jelley, R. O'Brien, and J. Silver, J. Phys. B **12**, 1665 (1979).

[36] M. Bitter, K. W. Hill, M. Zarnstorff, S. von Goeler, R. Hulse, L. C. Johnson, N. R. Sauthoff, S. Sesnic, K. M. Young, M. Tavernier *et al.*, Phys. Rev. A **32**, 3011 (1985).

[37] TFR Group, F. Bombarda, F. Bely-Dubau, P. Faucher, M. Cornille, J. Dubau, and M. Loulergue, Phys. Rev. A **32**, 2374 (1985).

[38] TFR Group, M. Cornille, J. Dubau, and M. Loulergue, Phys. Rev. A **32**, 3000 (1985).

[39] H. Hsuan, M. Bitter, K. W. Hill, S. von Goeler, B. Grek, D. Johnson, L. C. Johnson, S. Sesnic, C. P. Bhalla, K. R. Karim, F. Bely-Dubau, and P. Faucher, Phys. Rev. A **35**, 4280 (1987).

[40] P. Beiersdorfer, M. H. Chen, R. E. Marrs, M. B. Schneider, and R. S. Walling, Phys. Rev. A **44**, 396 (1991).

[41] J. Suleiman, H. G. Berry, R. W. Dunford, R. D. Deslattes, and P. Indelicato, Phys. Rev. A **49**, 156 (1994).

[42] A. J. Smith, P. Beiersdorfer, V. Decaux, K. Widmann, A. Osterheld, and M. Chen, Phys. Rev. A **51**, 2808 (1995).

[43] J. E. Rice, M. A. Graf, J. L. Terry, E. S. Marmar, K. Giesing, and F. Bombarda, J. Phys. B **28**, 893 (1995).

[44] V. Decaux, P. Beiersdorfer, S. M. Kahn, and V. L. Jacobs, Astrophys. J. **482**, 1076 (1997).

[45] B. J. Wargelin, S. M. Kahn, and P. Beiersdorfer, Phys. Rev. A **63**, 022710 (2001).

[46] M. R. Tarbutt, R. Barnsley, N. J. Peacock, and J. D. Silver, J. Phys. B **34**, 3979 (2001).

[47] P. Beiersdorfer, M. Bitter, D. Hey, and K. J. Reed, Phys. Rev. A **66**, 032504 (2002).

[48] V. Decaux, V. L. Jacobs, P. Beiersdorfer, D. A. Liedahl, and S. M. Kahn, Phys. Rev. A **68**, 012509 (2003).

[49] C. Biedermann, R. Radtke, and K. Fournier, Nucl. Instrum. Methods Phys. Res. Sect. B **205**, 255 (2003).

[50] J. K. Rudolph, S. Bernitt, S. W. Epp, R. Steinbrügge, C. Beilmann, G. V. Brown, S. Eberle, A. Graf, Z. Harman, N. Hell *et al.*, Phys. Rev. Lett. **111**, 103002 (2013).

[51] S. Schlesser, S. Boucard, D. S. Covita, J. M. F. dos Santos, H. Fuhrmann, D. Gotta, A. Gruber, M. Hennebach, A. Hirtl, P. Indelicato *et al.*, Phys. Rev. A **88**, 022503 (2013).

[52] J. E. Rice, M. L. Reinke, J. M. A. Ashbourn, C. Gao, M. M. Victora, M. A. Chilenski, L. Delgado-Aparicio, N. T. Howard, A. E. Hubbard, J. W. Hughes *et al.*, J. Phys. B **47**, 075701 (2014).

[53] D. B. Thorn, G. V. Brown, J. H. T. Clementson, H. Chen, M. Chen, P. Beiersdorfer, K. R. Boyce, C. A. Kilbourne, F. S. Porter, and R. L. Kelley, Can. J. Phys. **86**, 241 (2008).

[54] H. D. Dohmann, D. Liesen, and H. Pfeng, Z. Phys. A **285**, 171 (1978).

[55] P. Indelicato and E. Lindroth, Phys. Rev. A **46**, 2426 (1992).

[56] T. Mooney, E. Lindroth, P. Indelicato, E. G. Kessler, and R. D. Deslattes, Phys. Rev. A **45**, 1531 (1992).

[57] P. Indelicato, S. Boucard, and E. Lindroth, Eur. Phys. J. D **3**, 29 (1998).

[58] R. D. Deslattes, E. G. Kessler, Jr., P. Indelicato, L. de Billy, E. Lindroth, and J. Anton, Rev. Mod. Phys. **75**, 35 (2003).

[59] P. Amaro, C. I. Szabo, S. Schlesser, A. Gumberidze, E. G. Kessler, A. Henins, E. O. Le Bigot, M. Trassinelli, J. M. Isac, P. Travers *et al.*, Radiat. Phys. Chem. **98**, 132 (2014).

[60] B. L. Henke, E. M. Gullikson, and J. C. Davis, At. Data Nucl. Data Tables **54**, 181 (1993).

[61] C. I. Szabo, P. Amaro, M. Guerra, S. Schlesser, A. Gumberidze, J. P. Santos, and P. Indelicato, in *Proceedings of*

the 22nd International Conference on Application of Accelerators in Research and Industry, Ft. Worth, 2012, edited by F. D. McDaniel, B. L. Doyle, G. A. Glass, and Y. Wang, AIP Conf. Proc. No. 1525 (AIP, Melville, 2013), p. 68.

[62] C. I. Szabo, P. Amaro, M. Guerra, J. P. Santos, A. Gumberidze, J. Attard, and P. Indelicato, Phys. Scr. **2013**, 014077 (2013).

[63] See Supplemental Material at http://link.aps.org/supplemental/10.1103/PhysRevA.101.062505 for details on the method and figures.

[64] W. H. Press, B. P. Flannery, S. A. Teukolsky, and W. T. Vetterling, *Numerical Recipes: The Art of Scientific Computing*, 3rd ed. (Cambridge University Press, Cambridge, 2007).

[65] M. Trassinelli, Nucl. Instrum. Methods Phys. Res. Sect. B **408**, 301 (2017).

[66] U. von Toussaint, Rev. Mod. Phys. **83**, 943 (2011).

[67] R. Trotta, Contemp. Phys. **49**, 71 (2008).

[68] D. S. Sivia and J. Skilling, *Data Analysis: A Bayesian Tutorial*, 2nd ed. (Oxford University Press, Oxford, 2006).

[69] C. Gordon and R. Trotta, Mon. Not. R. Astron. Soc. **382**, 1859 (2007).

[70] J. P. Desclaux, Comput. Phys. Commun. **9**, 31 (1975).

[71] P. Indelicato and J. P. Desclaux, Phys. Rev. A **42**, 5139 (1990).

[72] P. Indelicato, O. Gorceix, and J. P. Desclaux, J. Phys. B **20**, 651 (1987).

[73] P. Indelicato and J. Desclaux, MCDFGME, a Multiconfiguration Dirac-Fock and General Matrix Elements Program (2005), http://kroll.lkb.upmc.fr/mcdf

[74] V. M. Shabaev, I. I. Tupitsyn, and V. A. Yerokhin, Phys. Rev. A **88**, 012513 (2013).

[75] V. M. Shabaev, I. I. Tupitsyn, and V. A. Yerokhin, Comput. Phys. Commun. **189**, 175 (2015).

[76] V. A. Yerokhin, Phys. Rev. A **97**, 052509 (2018).

[77] I. P. Grant, Adv. Phys. **19**, 747 (1970).

[78] I. P. Grant and H. M. Quiney, Adv. At. Mol. Phys. **23**, 37 (1988).

[79] P. Indelicato, Phys. Rev. A **51**, 1132 (1995).

[80] V. M. Shabaev, Theor. Math. Phys. **63**, 588 (1985).

[81] V. Shabaev and A. Artemyev, J. Phys. B **27**, 1307 (1994).

[82] V. M. Shabaev, Phys. Rev. A **57**, 59 (1998).

[83] J. Li, C. Nazé, M. Godefroid, S. Fritzsche, G. Gaigalas, P. Indelicato, and P. Jönsson, Phys. Rev. A **86**, 022518 (2012).

[84] J. M. Sampaio, F. Parente, C. Nazé, M. Godefroid, P. Indelicato, and J. P. Marques, Phys. Scr. **2013**, 014015 (2013).

[85] G. Audi, A. H. Wapstra, and C. Thibault, Nucl. Phys. A **729**, 337 (2003).

[86] I. Angeli, At. Data Nucl. Data Tables **87**, 185 (2004).

[87] I. Angeli and K. P. Marinova, At. Data Nucl. Data Tables **99**, 69 (2013).

[88] J. P. Santos, J. P. Marques, F. Parente, E. Lindroth, P. Indelicato, and J. P. Desclaux, J. Phys. B **32**, 2089 (1999).

[89] J. P. Santos, G. C. Rodrigues, J. P. Marques, F. Parente, J. P. Desclaux, and P. Indelicato, Eur. Phys. J. D **37**, 201 (2006).

[90] M. C. Martins, J. P. Marques, A. M. Costa, J. P. Santos, F. Parente, S. Schlesser, E. O. Le Bigot, and P. Indelicato, Phys. Rev. A **80**, 032501 (2009).

[91] P. Mohr, Ann. Phys. (NY) **88**, 26 (1974).

[92] P. J. Mohr, Phys. Rev. A **46**, 4421 (1992).

[93] P. J. Mohr and Y.-K. Kim, Phys. Rev. A **45**, 2727 (1992).

[94] P. Indelicato and P. J. Mohr, Phys. Rev. A **46**, 172 (1992).

[95] E.-O. Le Bigot, P. Indelicato, and P. J. Mohr, Phys. Rev. A **64**, 052508 (2001).

[96] P. J. Mohr and G. Soff, Phys. Rev. Lett. **70**, 158 (1993).

[97] P. Indelicato and P. J. Mohr, Hyperfine Interact. **114**, 147 (1998).

[98] V. A. Yerokhin, P. Indelicato, and V. M. Shabaev, Phys. Rev. Lett. **91**, 073001 (2003).

[99] V. Yerokhin, P. Indelicato, and V. Shabaev, Eur. Phys. J. D **25**, 203 (2003).

[100] V. A. Yerokhin, P. Indelicato, and V. M. Shabaev, Phys. Rev. Lett. **97**, 253004 (2006).

[101] V. A. Yerokhin, P. Indelicato, and V. M. Shabaev, Can. J. Phys. **85**, 521 (2007).

[102] V. A. Yerokhin, P. Indelicato, and V. M. Shabaev, Phys. Rev. A **77**, 062510 (2008).

[103] V. A. Yerokhin, Phys. Rev. A **80**, 040501(R) (2009).

[104] V. A. Yerokhin, Eur. Phys. J. D **58**, 57 (2010).

[105] P. Indelicato, Phys. Rev. A **87**, 022501 (2013).

[106] P. Indelicato, F. Parente, and R. Marrus, Phys. Rev. A **40**, 3505 (1989).

[107] P.-O. Löwdin, Phys. Rev. **97**, 1474 (1955).

[108] P. Indelicato, Hyperfine Interact. **108**, 39 (1997).

[109] G. Howat, T. Åberg, and O. Goscinski, J. Phys. B **11**, 1575 (1978).

[110] M. F. Gu, Can. J. Phys. **86**, 675 (2008).

[111] F. F. Goryaev, L. A. Vainshtein, and A. M. Urnov, At. Data Nucl. Data Tables **113**, 117 (2017).

[112] L. A. Vainshtein and U. I. Safronova, At. Data Nucl. Data Tables **21**, 49 (1978).

[113] A. M. Costa, M. C. Martins, F. Parente, J. P. Santos, and P. Indelicato, At. Data Nucl. Data Tables **79**, 223 (2001).

[114] J. Nilsen, At. Data Nucl. Data Tables **38**, 339 (1988).

[115] V. A. Yerokhin and A. Surzhykov, J. Phys. Chem. Ref. Data **47**, 023105 (2018).

[116] C. P. Bhalla and T. W. Tunnell, J. Quant. Spectrosc. Radiat. Transfer **32**, 141 (1984).

[117] M. H. Chen, At. Data Nucl. Data Tables **34**, 301 (1986).

[118] A. D. Whiteford, N. R. Badnell, C. P. Ballance, S. D. Loch, M. G. O'Mullane, and H. P. Summers, J. Phys. B **35**, 3729 (2002).

[119] U. I. Safronova and A. S. Shlyaptseva, Phys. Scr. **54**, 254 (1996).

[120] M. H. Chen, B. Crasemann, and H. Mark, Phys. Rev. A **24**, 1852 (1981).

[121] P. Indelicato and P. J. Mohr, Phys. Rev. A **63**, 052507 (2001).

[122] R. Brun and F. Rademakers, Nucl. Instrum. Methods Phys. Res. Sect. A **389**, 81 (1997).

[123] I. Antcheva, M. Ballintijn, B. Bellenot, M. Biskup, R. Brun, N. Buncic, P. Canal, D. Casadei, O. Couet, V. Fine *et al.*, Comput. Phys. Commun. **180**, 2499 (2009).

[124] I. Antcheva, M. Ballintijn, B. Bellenot, M. Biskup, R. Brun, N. Buncic, P. Canal, D. Casadei, O. Couet, V. Fine *et al.*, Comput. Phys. Commun. **182**, 1384 (2011).

[125] B. Gough, *GNU Scientific Library Reference Manual*, 3rd ed. (Network Theory Ltd., Boston, 2009).

[126] R. Piessens, E. de Doncker-Kapenga, C. W. Überhuber, and D. K. Kahaner, *Quadpack: A Subroutine Package for Automatic Integration*, Springer Series in Computational Mathematics Vol. 1 (Springer, Berlin, 2012).

[127] M. Guerra, P. Amaro, C. I. Szabo, A. Gumberidze, P. Indelicato, and J. P. Santos, J. Phys. B **46**, 065701 (2013).

[128] A. Kramida, Y. Ralchenko, J. Reader, and N. A. Team, NIST Atomic Spectra Database, version 5.7.1 (NIST, Gaithersburg, 2019), available at https://physics.nist.gov/asd.

[129] J. E. Rice, K. B. Fournier, J. A. Goetz, E. S. Marmar, and J. L. Terry, J. Phys. B **33**, 5435 (2000).

[130] S. Bernitt, G. V. Brown, J. K. Rudolph, R. Steinbrugge, A. Graf, M. Leutenegger, S. W. Epp, S. Eberle, K. Kubicek, V. Mackel *et al.*, Nature (London) **492**, 225 (2012).